This is to certify that the

thesis entitled

Three-dimensional Elastic Seismic Response
of Deck-type Arch Bridges

presented by

Robert Joseph Millies

has been accepted towards fulfillment
of the requirements for

M.S. degree in Civil Engineering

R. K. Wen
F. J. Hatfield

Major professor

Date 4/2/92

THREE-DIMENSIONAL ELASTIC SEISMIC RESPONSE OF DECK-TYPE ARCH BRIDGES

By

Robert Joseph Millies

A THESIS

Submitted to
Michigan State University
in partial fulfillment of the requirements
for the degree of

MASTER OF SCIENCE

Department of Civil and Environmental Engineering

1992

ABSTRACT

THREE-DIMENSIONAL ELASTIC SEISMIC RESPONSE OF DECK-TYPE ARCH BRIDGES

By

Robert Joseph Millies

A study of the lateral stiffness of the end towers of a bridge was conducted using computer modelling. The bridge model is symmetric, consisting of geometrically nonlinear curved beam elements for parabolic ribs with cross-bracing and a trussed deck. Three span lengths of 200, 600 and 1000 feet were studied. The 1940 El Centro ground motion in 3 directions was used.

The tower lateral stiffness essentially affected the out-of-plane response only. For short spans, this response contributed significantly to the rib stresses. Accordingly, an increase in the tower stiffness increases the rib stress in the 200 ft. span. For the longer spans, the tower stiffness had small affects on the rib stresses because the lateral responses were small. However, the displacements at the towers were significantly decreased by a tower stiffness increase. Lateral tower stiffness of the order of 50% relative to that of the rib system seems appropriate for design purposes.

To my dad (Robert H.), mom (Maureen), sisters,

"The Real Men of Pittsford", friends &

my future wife (whomever she may be)

for their incalculable support towards

my every endeavor, thanks.

ACKNOWLEDGEMENTS

At this time I would like to acknowledge with sincere appreciation the opportunity given by Dr. Robert K. L. Wen, Professor of Civil Engineering, Michigan State University, to conduct this study. His role as thesis advisor, as well as, engineering scholar, mentor, general counselor and friend is appreciated and will not be forgotten. Without Dr. Wen, this study would not have been possible.

I would also like to thank the National Science Foundation for the financial support. I would like to thank my committee members, the Civil and Environmental Engineering Department and Case Computing Center at Michigan State University. Finally, I would like to thank God for this opportunity and for the family and friends He has given me.

TABLE OF CONTENTS

TABLE OF CONTENTS (Continued)

LIST OF TABLES

LIST OF FIGURES

LIST OF FIGURES (continued)

Figure Page

LIST OF FIGURES (continued)

Chapter I

Introduction

According to the theory of plate tectonics, the earth's surface consists of a number of plates which are constantly in motion. As these plates move against each other, strain energy is accumulated in them until, eventually, the material fails, sending off shock waves. This is the cause of most earthquakes. The San Fernando earthquake that occurred in 1971 caused much damage to bridges. Since then, the engineering field has given much time and effort to the study of earthquakes and how to build stronger, safer structures to withstand earthquakes. This study is a step towards a better understanding of the effects of earthquakes on a particular type of structure, steel arch bridges.

Thakkar and Arya [9] had reported the linear response of single arch ribs to in-plane seismic motions. Using a simple model of lumped flexibility and lumped mass, Raithel and Franciosi [8] illustrated the elastic vertical vibrations of arches caused by horizontal seismic excitations. The decrease of the natural frequencies due to compression in the arch was also illustrated.

The linear behavior of deck arch bridges subjected to realistic ground motion in three dimensional space has been discussed by Dusseau and Wen [2,3]. Lee [5] has presented a method of analysis for the geometrically nonlinear and inelastic responses of arch bridges. A general computer program was developed and illustrative applications were given.

The above computer program was modified to include a more effective type of nonlinear curved beam elements [13] and used to produce application oriented data for in-plane response [12].

The objective of this thesis is to study (using the program) the seismic response from a designer's point of view, chiefly in the consideration of the lateral stiffness needed for the end towers of the bridge. In the course of the work, an appreciable amount of effort was expended in adapting the modified program for design studies in a three-dimensional setting.

The program was modified to include the automatic generation of the nodal coordinates for the cross beams between the ribs. The time step-size (used in the dynamic analysis) input was modified so as to be a function of the fundamental period. A Lagrange interpolation function was implemented to determine the ratio of the two principal moments of inertia of the rib cross section as a function of span length. This ratio then allowed for the computation of the other geometrical properties.

This study concentrates on the role of the end towers which are the "bents" at the bridge ends rising from the arch support level to support the deck, see Figure 1. They are analogous to the towers of suspension bridges, in that their actions under gravity loads are a relatively simple one of transmitting vertical loads down to the foundation through compression of the vertical members.

When the bridge is subjected to lateral (normal to the planes of the arches) loads, such as wind or seismic loads, the designer needs to decide on a scheme for the transmission of the loads to the foundation. Assuming that a horizontal shear connection is provided between the deck and the arch ribs (usually at the crown), the towers and the ribs partake in the lateral load transference. Such action obviously depends on the lateral stiffness of the tower relative to that of the arches.

In the case of static loads (wind load is usually treated as such) this relative stiffness would play the major role in determining the proportioning of the given total design lateral loads to the ribs and the end towers. It is well-known that the seismic design load on a structure depends on its natural frequencies. In the case of seismic loading (due to lateral ground motion), the stiffness would have the additional effect of actually defining the loading itself as the stiffness affects the out-of-plane natural frequencies of the structure.

The main purpose of this thesis is to elucidate the preceding observation using computer analysis. The computer model and the parameters of the systems studied are described in Chapter 2. The results of the study are presented in Chapter 3. A summary and conclusions are given in Chapter 4.

Chapter II

Modelling and Parameters

This chapter discusses the modelling system and the parameters. In the first section, the bridge system studied is discussed. In the second section, a discussion of the parameters of the system is given.

2.1 Bridge System Considered

Herein, the components of the bridge and their action are described. The assumptions of the system studied are given, followed by a summary of the analysis.

2.1.1 Description of Bridge Model

A real arch bridge containing a multitude of components is a system with a large number of degrees of freedom (d.-o.f.). It was necessary, due to resource limitations, to use a model that had as few d.o.f. as feasible on the one hand and yet could still be expected to capture the essential feature of the prototype on the other. This is particularly true here since the analysis is nonlinear and consequently requires more computing resources.

In an arch bridge, the major structural components are the arch ribs which are the main object of this study. Thus, in formulating the bridge model, the subsystem of the ribs is given greater precision than the deck and the end towers. For the latter, the model would provide only the interaction between them and the ribs. The modelling for the deck and tower is not intended to reflect the internal behavior of the deck subsystem or the tower subsystem at their component level.

The model used is shown in Figure 1. It consists of a twin-rib system: a rib in front and a rib in back. The arch is parabolic in shape. The ribs consist of curved beam elements. The ribs are braced together to form a unit by "cross beams" and cross-bracing (X-bracing). The cross beams which are perpendicular to the planes of the ribs are modelled by straight beam elements. The X-bracing run in diagonal directions between the cross beams and are modelled as truss elements.

The main feature of the 3-D system when compared with the 2-D in-plane system, is the out-of-plane torsional bending behavior. To strengthen the torsional response, the rib bracing could have X-bracing along the top faces of the ribs and another X-bracing along the bottom faces. This would form a "torsional box" as shown in Figure 2a. Since it is cumbersome to include two layers of X-bracing in the model, a model is used as shown in Figure 2b. To simulate the relatively large torsional stiffness of the "torsional box" in Figure 2a, the value of the torsional stiffness of the individual ribs in Figure 2b could be increased.

The deck system which includes "stringers", "X-bracing" and "cross beams," is represented entirely by truss elements. It is connected to the end towers and to the crown of the arch. The in-plane bending stiffness of the deck stringers are neglected. Similarly, the deck in the model does not contribute significantly to the torsional stiffness of the system. However, the deck as a horizontal truss can resist substantial bending in the horizontal plane.

The deck and ribs are connected by "columns" modelled as truss elements. Truss elements are also used for X-bracing for the deck.

Each end tower is represented by a vertical bent consisting of four truss elements; two vertical elements and two diagonal elements (the stiffness of which essentially defines the lateral stiffness of the tower).

Lastly, the support conditions are as follows. For the rib ends, all d.o.f. are restrained except rotation about the Z-axis (i.e. rotation in the plane of the arch). The towers are hinged at their lower ends and ("pin-") connected to the deck at the upper ends. As mentioned previously, the deck is also directly hinged to the ribs at the crown.

2.1.2 Assumptions of the System Studied

The system studied is symmetric about two vertical planes: one containing the crown and parallel to the end towers; the other is in between the two planes of the two ribs. The bridge, as a whole, was modeled. The mass of the deck and that of the arch is distributed uniformly along their horizontal projection. All rib elements have the same cross-section. Likewise, all elements within a group (e.g. X-beams, or rib X-bracing) have the same cross-sectional properties.

2.1.3 Discussion of Analysis

The computer program used for the study and the method of analysis on which it was based are essentially those as described by C. M. Lee [5]. There, the truss elements and straight beam elements were linearly elastic. For the curved beam elements both geometric nonlinearity and plasticity were allowed. The masses were lumped at the nodes. Rayleigh damping was assumed. Two coordinate systems were used for the "Global Stiffness Matrix": Curvilinear coordinate system for the arch nodes and the common Cartesian coordinate system for the deck nodes.

The computation of the seismic response would consist of two steps: 1. A linearly elastic static analysis was made for the dead load; and 2. The results were used as the initial conditions to compute the seismic response. For the latter analysis, the Newmark β-method ($\beta = 1/4$) of numerical integration was used for the time domain, and the Newton-Raphson method was used to deal with the nonlinearity content of the problem.

The computer program used in this study is a modification of the one described above. The modifications include the following:

1. A new nonlinear curved beam element [13] is

used to replace the old one. The new element makes it possible to compute the resistance much more accurately.

2. The dual coordinate systems described previously is replaced by a single Cartesian system (X, Y and Z denote global coordinate system; x, y and z denote member coordinate system). Although this would incur more computing, it is more than compensated by the avoidance of confusion to the user of the program.

3. Straight beams with general global geometry are allowed. (Previously, in order to save computing time, straight beams were fixed as horizontal or vertical members.)

4. The two separate inputs for computer solutions (dead load - static, and then seismic - dynamic) are combined into one computer run.

5. The eigensolution values needed for the specification of the Rayleigh damping is also incorporated directly into the analysis. (Previously, this was done separately.)

6. As a consequence of 5. above, the size of the time increment used in the numerical integration is made a fraction of the computed fundamental period (instead of a preset constant).

7. The stiffness of the rib system is calculated

using F = kz. A uniformly distributed load (F) in the Z-direction is applied to the deck and ribs and the corresponding crown displacement (z) is measured. The stiffness (k) is equal to the total load applied divided by the displacement. This value of the rib lateral stiffness multiplied by a ratio of end tower lateral stiffness to rib lateral stiffness will give the lateral stiffness of the end towers. The lateral stiffness of the end tower is defined as the load applied at the top of the end tower in the Z-direction to cause a unit displacement thereat.

8. A number of convenient measures are added for engineering studies (such as this one). They include the automatic generation of input data such as mass and stiffness quantities based on the parameters defined in the next section as well as the "post processing" of data such as searching for the maximum of the response values.

2.2 Parameters

The following section discusses the parameters chosen to define the system being considered. Estimations of their ranges, "central values" and those used in the study are also presented.

2.2.1 Parameters Associated with the In-Plane Behavior

There are ten parameters that are associated with the bridge in-plane behavior and are given in Table 1. The first column lists the parameters; the second column, their ranges; the third, the values used in this study.

The parameters associated with the in-plane behavior are as follows: H/L is the rise (H) to span length (L) ratio; L/r_y is the "slenderness ratio", representing the span length over the radius of gyration about the rib's local y-axis (the local y-axis of curved beam cross section is its principal axis normal to the plane of the arch and the local x-axis is the other principal axis); G is equal to $MgL^3/(EI_{yr})$ (in which M is the total mass per foot of span length, L, g is the gravitational acceleration, E is the Young's modulus and I_{yr} is the moment of inertia about y); M_r/M is the mass of the rib over the total mass; N is the number of panels; ξ is the critical damping coefficient for the first two modes; and the ratio c_y/r_y in which c_y is one half of the depth of the rib cross-section; and x_g and y_g are the accelerations in the X- and Y-directions, respectively.

2.2.2 Additional Parameters Associated with Out-of-Plane Behavior

The additional parameters associated with out-of-plane behavior are also listed in Table 1. They include: W, the width; I_{xr}/I_{yr}, the moment of inertia about x-axis of the rib to the moment of inertia about the y-axis of the rib; c_x/r_x, in which c_x is the distance in the rib local x-direction from the neutral axis to the extreme fibers (or one half of the width) and r_x is the radius of gyration about the x-axis of the rib; A_x/A_r, in which A_x is the cross-sectional (x-sectional) area of the rib X-bracing and A_r is the x-sectional area of the rib; A_b/A_r, in which A_b is the x-sectional area of the cross beams; I_{yb}/I_{yr} in which I_{yb} is the moment of inertia about the y-axis of the cross beam; I_{xb}/I_{yb} in which I_{xb} is the moment of inertia about the x-axis for the cross beam; K_{tb}/I_{yb} in which K_{tb} is the torsional constant of the cross beam; α is the ratio of the lateral stiffness of the end tower to the lateral stiffness of the braced system of the two ribs; A_s/A_r in which A_s is the x-sectional area of the deck stringers; and z_g is the ground acceleration in the global Z-direction.

The columns (between the deck and the ribs) and the X-bracing of the deck are represented by essentially rigid truss members. These elements are not formally regarded as parameters of the model.

By a review of the properties of several existing bridges [7] [14], estimates of the range and/or representative values of the parameters are listed in column two of Table 1. For the present study, the values of the parameters used are given in column three of the same table.

The ground motions of the 1940 El Centro earthquake are shown in Figure 3. The variables x_g, y_g and z_g are used to represent, respectively, the north-south, vertical and eastwest components of the El Centro ground accelerations. The magnitude of the ground accelerations were not scaled throughout this study.

The program has the capability of using a linear, geometrically nonlinear or "linearized" model for the dynamic analysis. The "linearized" model employs the nonlinear model for the initial dead load solution and the subsequent response to seismic motion would be calculated based on a linear analysis using the tangent stiffness of the structure under dead load. A comparison of the program results using linear, nonlinear or linearized analysis was made and is shown in Figures 4 - 6. These figures show the time history displacements of an arch quarter point. From the figures, it is seen that there is a relatively large difference between the linear and nonlinear case and the linear and linearized case; but there is not a noticeable difference between the nonlinear and linearized case. Therefore, the method of linearized analysis was chosen for use in this study.

CHAPTER III

RESULTS

This chapter presents and discusses the results obtained for the study. In the first section of this chapter, the inter-rib bracing parameters are determined. In the second section, the roles of the end towers are investigated.

3.1 Determination of Inter-Rib Bracing Parameters

The inter-rib bracing consists of cross beam members and cross-bracing (X-bracing) truss members placed between the ribs as shown in Figure 1. Since this study focuses on rib response, the deck was made essentially rigid. Because of the limited role of the inter-rib bracing members, and with a view to minimizing the number of parameters, a study was made to fix the numerical values of the parameters representing the inter-rib bracing.

With the proper bracing, the two ribs would act as a unit. An "optimal" or "efficient" amount of bracing material to enable this action needs to be determined. For the beam, this was interpreted to mean that an additional increase beyond that amount would not have a major effect on the fundamental out-of-plane frequency. For the X-bracing, this was interpreted to mean that an additional increase would have little effect on the magnitudes of the member forces caused by a lateral load.

The cross-sectional properties of the beams are area (A_b), moment of inertia about y- and x-axis (I_{yb} and I_{xb}), and torsion constant (K_{tb}). The X-bracing as truss members has only the area property (A_x) to define their cross-sectional properties. The parameters used for this study are A_b/A_r (the area of the beam to that of rib), I_{yb}/I_{yr} (the beam moment of inertia about the y-axis to the rib moment of inertia about the y-axis), I_{xb}/I_{yb} (the beam moment of inertia about the x-axis to the beam moment of inertia about the y-axis), K_{tb}/I_{yb} (the torsional constant to the moment of inertia about the y-axis for the beam) and A_x/A_r (the X-bracing area to the rib area). Values for the above parameters were determined as follows.

First, as indicated by an existing bridge, $K_{tb}/I_{yb} = I_{xb}/I_{yb} = 1.0$ seemed reasonable. After some initial trial-and-error, it was decided to use:

$$I_{yb}/I_{yr} = 0.05$$

$$A_b/A_r = 0.10$$

$$A_x/A_r = 0.04$$

In support of the above choices Figure 7 shows the effect of I_{yb}/I_{yr} on the fundamental out-of-plane natural frequency. It may be seen that the frequency began levelling off, approximately, at $I_{yb}/I_{yr} = 0.05$. Figure 8 shows the fundamental out-of-plane natural frequency is not influenced by a variation of A_b/A_r. Figure 9 shows the variation of the rib X-bracing member forces as a factor of A_x/A_r. It is seen that the member force increases rapidly with small values of A_x/A_r. However, the increase levelled off after it reached 0.04.

3.2 Role of Tower Lateral Stiffness

This section is concerned with the effects of the end towers, its lateral stiffness in particular. The first part presents some general comments. In part two, the sequencing of the in-plane and out-of-plane modes is considered. In part three, the influence of the tower lateral stiffness on the stress ratio in the arch rib is discussed. In part four, the influence of the tower lateral stiffness on the deck lateral displacement is discussed. In part five, the influence of the tower lateral stiffness on the lateral load proportioning between the arch ribs and the towers is discussed. And in part six, static wind stresses are compared with dynamic seismic stresses.

3.2.1 General Comments on the Lateral Stiffness in Tower

Let the ratio of the lateral stiffness of the tower to the lateral stiffness of the braced arch ribs be denoted by α. The lateral stiffness of the rib and tower is defined in Chapter 2.1.3. The parameter α influences two aspects of the bridge response: 1.) the local tower displacements, and 2.) the overall bridge response to lateral ground motion as it affects the out-of-plane natural frequencies.

The total dynamic response, R, may be expressed as $R = R_{ST} * AF$. R_{ST} is the static response; it depends on the stiffness of the structure. AF denotes "amplification factor" which depends mainly on the natural frequency. As the structural stiffness is increased, R_{ST} is decreased, but the corresponding change in the natural frequency may increase or decrease AF. The nature of dependence of AF on the natural period of vibration is illustrated in Figure 10, which is the acceleration response spectrum given in the AASHTO Seismic Design Specifications for Bridges.

In order to aid in the understanding of the dynamic stress distribution in the arch ribs due to three dimensional excitations, the stresses under static loads for lengths of 200 ft. and 600 ft. are discussed here. For these span lengths, the stresses for three loading cases are presented in Figure 11 and 12, respectively. The cases are static loadings of 0.3g applied through the nodal masses separately in the X-, Y- and Z-directions.

Under x-loading for span length = 200 and 600 ft., the maximum static stress occurs in the area of the quarter points of the arch (1/4 of the span length, from the end points) and is a minimum at the crown of the arch and the supports (ends). The x-loading produces the largest stress when compared to y- and z-loadings.

Under y-loading for span length = 200 and 600 ft., the maximum stress occurs at the middle of the arch and minimum at the supports. There is a difference on the order of 10 between the x-loading and y-loading.

Under the z-loading for span length = 200 and 600 ft., the distribution of stresses resembles an inversion of that due to the x-loading. The maximum stress occurs at the supports and crown of arch, while the minimum occurs at the quarter points. The maximum stresses due to z-loading are approximately one-third the stresses due to x-loading and approximately three times the stresses due to y-loading.

The distribution of the stresses due to y-loading differs from the known stress distribution due to a uniformly distributed vertical load on the horizontal projection of the arch (having a uniform cross-section)in which the maximum stress occurs at the supports. And the only type of stress involved is a compressive stress. But in this model, the loading is not uniform; the vertical load from the deck is transferred through the columns to the rib and is applied as concentrated loads. These concentrated loads not only produce compressive forces but also bending moments. The moment due to bending is the largest at the crown and therefore causes large bending stress to occur, despite the relatively small compressive stress involved.

Table 2 shows the distribution of stresses for individual members. The stress is chosen from the I-node only of each curved beam member of the rib and is calculated using:

$$\text{stress} = |P/A| + |M_y/S_y| + |M_x/S_x| \ldots\ldots\ldots\ldots (1)$$

where: $|\;|$ denotes absolute value,

P = compressive force

A = cross-sectional area

M_y, M_x = the bending moment about y-axis and x-axis, respectively

S = the section modulus.

The stresses listed occurred in the specified member under the given static loading, i.e., x-, y- or z-loading of 0.3g each. The member number of the front rib is listed, and the number next to it in parenthesis is the member in the back rib, indicating symmetry between the front and back ribs. The SAM, SYM and SXM headings pertain to the ratio of stress due to axial force or bending moments about the y- and x-axis, respectively, divided by the total stress:

$$SAM = |P/A|/\Sigma_{total}$$

$$SYM = |M_y/S_y|/\Sigma_{total}$$

$$SXM = |M_x/S_x|/\Sigma_{total}$$

where Σ_{total} represents the total stress.

SAM, SYM and SXM should always sum to one. For example, member 2, y-only (y-loading only) has a stress at the I-node of 3.01 ksi and that 57% of it comes from axial stress and 43% from bending about the y-axis.

The z-loading case is the only case that has significant values from each of SAM, SYM and SXM. The x- and y-loading cases have contributions to the total stress from SAM, SYM but not SXM. The stresses due to the x-loading case is governed by bending moment stresses at internal nodes, but at the supports, the stresses are due to axial force. As noted earlier, the support has a moment release about z-axis only.

3.2.2 Effect of α on the Sequencing of In-plane and Out-of-plane Normal Modes

The parameter α influences the eigen-solutions of the arch bridge. As α is varied for a given length, the sequencing of the in-plane and out-of-plane normal modes changes. In Table 3, these modes are listed for lengths of 200 ft., 600 ft., and 1000 ft. The letters "in" mean in-plane and the letters "out" mean out-of-plane, the number beside "in" or "out" is the frequency of that mode, in Hertz. The T_{in} and T_{out} values represent the period of the fundamental in-plane (a full wave-length in the X-Y plane) and fundamental out-of-plane (a half wave-length in the X-Z plane) modes, respectively. As can be seen, as α increases, the in-plane modes rise up in ranking and become more dominant. For the length = 200 ft. case, as α increases from 0.5 to 9.0, the difference between the fundamental periods of the in-plane and the out-of-plane increases. This is due to the fact that as α increases the stiffness in the lateral direction increases while the stiffness in the X-Y plane remains essentially unchanged. The increase in lateral stiffness moves the out-of-plane modes down in the "ranking" (the larger the value of the natural period, the higher the ranking). The same situation occurs for lengths of 600 ft. and 1000 ft. The fundamental mode for length = 600 ft. when α is 0.0 is out-of-plane and becomes in-plane when α is increased to 0.5. For the length = 1000 ft., the out-of-plane remains the fundamental mode for all values of α, but other than that the in-plane modes still rise in rank as α increases. Therefore, the selection of α for a given length can influence the type of modes of vibration that will be dominant in dynamic response.

3.2.3 Effect of α on Maximum Stress Ratio

The study of the maximum stress ratio (SR) that occurs within the ribs during an earthquake loading with all three (X,Y,Z) components is described in this section for varying α and lengths.

For length = 200 ft., the SR in the ribs varies from 2.54 to 3.86, see Figure 13. For length = 600 ft., the SR in the ribs varies from 2.5 to 3.7, see Figure 14, and for length = 1000 ft., the SR varies from 1.96 to 2.76, see Figure 15. In all three cases, the largest value of SR is near the ends. It is also observed that the shorter span is influenced more by the variation of α than the other span lengths.

For lengths = 200 ft. and 600 ft., the contribution of each component of the earthquake loading to SR is shown in Figures 16 and 17, respectively. The SR from the Z component is small for the length = 600 ft. case, and contributes very little to the stress when all three ground motions, X, Y and Z, are considered.

This is not the case for length = 200 ft. In this case the response to the Z component of the earthquake loading is much larger. An explanation for the difference may be found in Figure 10. It may be seen that for the 600 ft. span, with T_{out} (α = 0.1) = 3.42 s, the spectral response is relatively low (approximately 0.22). For the 200 ft. span, with T_{out} (α = 0.1) = 1.11 s, the spectral response is relatively high (approximately 0.45).

The maximum SR as a function of α, for length = 600 ft., is shown in Figure 18. The largest maximum SR that occurs is approximately 3.90 when α = 1.0. But is only about 5% more than the minimum. For length = 200 ft, see Figure 19, the largest maximum SR occurs at a larger α, specifically 3.0, and it is about 18% more than the minimum. Opposite to the length = 200 ft. case is the length = 1000 ft. case, see Figure 20, its largest maximum SR occurs at a lesser α than the length = 600 ft. case, specifically 0.1. The maximum SR for length = 1000 ft. is about 5% more than the minimum.

One may also note that the value of the largest maximum SR decreases as the length increases, from approximately 4.3 to 3.9 to 2.9. This is due mainly to the variance of values of natural periods, and hence the AF values, for the different lengths.

Lastly, the linear and the linearized analyses results were compared, as shown in Figure 21. When α is close to zero, the largest difference between the two types of analyses occur when the length = 200 ft., and the difference between the two becomes smaller as the length increases.

3.2.4 Effect of α on Deck Lateral (Z-) Displacement

The effects of the variable α on the Z-displacement (D_z) of the deck is illustrated in Figure 22 for the case span length = 600 ft. The displacement D_z is directly influenced by the stiffnesses of the tower and the arch ribs. It is seen that the deck end displacement decreases as α increases. Conversely, the deck middle point displacement increases as α increases. It may be worth noting again that at the mid-span, the deck and the rib crown meet, and thus have equal displacements. Also, the displacement shape of the deck is concave for α = 0 and 0.1, while it is convex for α larger than 0.5. As the value of α changes from 0 to 0.5, there is about a 50% reduction in the displacement at the end of the deck, while there is about a 15% increase in the displacement at the middle of the deck.

For the case of length = 200 ft. see Figure 23. The displacements vary much less from the end to the middle than for the case of the 600 ft. span, but the shapes still indicate a single curvature, either concave or convex. There is a large difference between α = 0 and 0.1, approximately a 50% reduction in D_z. This is probably due to the change in the frequency response via natural periods of vibration.

In Figure 24, the behavior of the deck's displacement for the case of length = 1000 ft. is shown to be quite similar to the length = 600 ft. case for approximately a 50% reduction in the displacement at the ends of the deck. At the middle of the span, a general decrease of D_z occurs with increasing the value of α past 0.5. One fact is worth noting. In Figure 24, D_z increased at all points when α was increased from 0 to 0.1. This is contrary to the behavior of other lengths for the same α range. It was probably due to a change in the frequency response of the structure. The natural period of the structure changed with an increase in α. An explanation can be given, similar to above, using Figure 10. After α was increased beyond 0.1, the D_z started to decrease at the ends, indicating that the increase in the static effect of the tower stiffness becomes dominate.

A comparison of the D_z for the three different lengths shows that the largest D_z occurs for length = 200 ft. when α = 0, the other two lengths, 600 ft.and 1000 ft., are very similar. At the middle of the span, the largest D_z occurs when the length = 600 ft. and α = 1.

The maximum value of the ratio of the maximum tower Z-displacement to the maximum arch crown Z-displacement (D_{tr}) is shown in Figures 25 - 27 as a function of α for the three span lengths. Since the rib D_z does not vary much, the variation of D_{tr} would be due mainly to variation in the tower displacement. For lengths = 600 ft. and 1000 ft. (Figs. 26 & 27), the curves sharply drop as α is increased from 0.0 to 2.0. The graph for the length = 200 ft. case (Figure 25) does not show as sharp a drop but does show a considerable decrease in the D_{tr} with α. These figures also suggest that for an α value as little as 0.5, the D_{tr} decreases approximately 62% for lengths = 600 ft. and 1000 ft. For the length = 200 ft. case, the decrease in D_{tr} of approximately 50% is associated with a value of 3.8 (derived from interpolation from figure 25) for α. The large difference between the lengths = 200 ft. and 600 ft (and 1000 ft.) is probably due to the fact that with the same width, the shorter bridge has a larger "depth-to-span ratio" with respect to the lateral loading than the longer bridge. Also, since the other properties of the deck were constant for each length, the deck became stiffer for the span length = 200 ft. case and therefore forced the tower and ribs to displace more uniformly. This uniformity demand by the deck caused the decrease in D_{tr} to be smoother than the other lengths.

The linear and linearized analyses for the maximum D_{tr} as a function of α were compared and is shown in figure 28. It is shown that there is very little difference between the two types of analyses.

3.2.5 Effect of α on Lateral Load Distribution

The total lateral load applied to the arch bridge, is transferred to the supports by the ribs and the towers. Therefore, the parameter α (tower stiffness to rib stiffness) influences the amount of force in the Z-direction, Z-force, that is taken by the towers and ribs. For α = 0, all the lateral load will be taken by the ribs, since the towers do not have any lateral stiffness for resisting lateral loads. Figure 29 shows, for the three different span lengths, the ratio of the Z-force through a single tower to the Z-force through the rib system (α_F) as a function of α.

For small values of α (approximately 0.1), the α_F is similar (0.1) as would be expected, but as α increases α_F does not respond linearly as one might think. An increase in the tower stiffness does not result in a corresponding increase in the tower Z-force. The magnitude of α_F is less as the length is increased. For length = 1000 ft. case, α_F levels off with increasing α starting at approximately α = 1.0. For the length = 600 ft., α_F levels off at approximately α = 2.0. For the length = 200 ft. case, the response of α_F to α is not the same as the other lengths, it does not have a distinct leveling-off point, but the rate of increase does decrease. For the 200 ft. bridge, an optimal value for α might be selected as 3.0.

For each length, when α is increased the trend of increasing α_F is similar but the magnitude of α_F is different. The magnitude of α_F decreases as the length of the bridge increases. This suggests that of the total lateral load that is created from the earthquake's displacement, the amount transferred to the towers decreases with length relative to the load transferred through the ribs.

In Figure 30, the values of α_F using linear and linearized are graphed as a function of α. The difference between the two types of analyses is small.

3.2.6 Effect of α on Seismic and Wind Stresses

The wind stresses and seismic stresses are compared here to relate the two considerations in design. Given a location for a bridge, the governing design lateral load is generally based on either a wind load or an earthquake, depending on which is more severe.

In this section, the wind load stresses are compared to seismic stresses. The wind load applied to the bridge was calculated according to the AASHTO bridge specifications [14]. The specifications state that for an arch bridge use a wind load of 75 psf applied to the windward side of the bridge. The windward side is the XY-plane of the bridge. The surface area was estimated as twice the surface area of the arch. The lumped wind load at each node was then calculated, in terms of gravity (g), to be 0.125g times the nodal mass.

The stresses due to wind and seismic input (Z-direction only) are shown in Table 4. The members with the maximum stress due to wind loading are located nearest the supports. According to Table 2 for member 1, the stresses are composed of 65% axial and 35% bending about the x-axis. The members with the maximum stress due to seismic loading are located near the crown of the arch. According to Table 2, these stresses are composed of 70% bending about the y-axis, 15% bending about the x-axis and 15% axial.

In Table 4, the symbol "1/4" represents the stress in the arch at the quarter point (which happens to be not the maximum). It is observed that for larger spans, the wind stress governs; for shorter spans, the seismic stress governs. Under the wind loading, the stresses tend to decrease as α increases. Under the seismic loading, the opposite occurs when the length = 200 ft. as α increases, the stress increases. For lengths = 600 ft. and 1000 ft., the seismic stresses do not change much with α and the direction of change is erratic.

The ratio SWR, the seismic stress to the wind stress ratio, varies with length and α as shown in Figure 31. For length = 1000 ft., it is seen that wind stresses are larger than seismic stresses. The SWR values range from 0.19 at α = 0.1, to 0.25 at α = 3.0. For length = 600 ft., the wind stress is larger at α = 0.1, but when α = 0.5 or larger, the seismic stress is larger. For length = 600 ft., SWR ranges from 0.74 at α = 0.1, to 1.77 at α = 8.0. For length = 200 ft., the seismic stress dominates for all α's. The SWR ranges from 2.65 at α = 0.1 to 17.59 at α = 8.0.

Figure 31 can be used as an aid in designing arch bridges. It pertains to the El Centro earthquake with a magnitude of 7 measured on the Richter scale. It is, in all probability, the largest earthquake that will occur in the United States. The spectral response of El Centro is very similar to Figure 10. For application of these results to a particular site with a different seismicity, the designer can scale accordingly. Considering this, the seismic response coefficienct, C_s, is calculated (according to AASHTO) in the following manner:

$$C_s = 1.2*Ac*S/T_m^{2/3} \quad \text{.....................} (2)$$

where Ac = the ground acceleration coefficient; S = the dimensionless for the soil profile characteristics of the site; and T_m = the period of the bridge.

For El Centro, Ac = 0.4 and S = 1, therefore, scaling may proceed as:

$$SF_{site} = (AS)_{site}/(AS)_{El\ Centro} \quad \text{...............} (3)$$

or,

$$SF_{site} = (AS)_{site}/0.4 \quad \text{....................} (4)$$

The seismic stresses may then be multiplied by SF_{site} (scaling factor) to obtain the stresses that may occur at the site due to a design earthquake. The design should then be checked to determine if the wind or seismic load governs.

Chapter IV

Summary & Conclusion

4.1 Summary

This study is concerned with seismic effects on deck-type arch bridges in three dimensional space. The focus of the study was on the influence of the lateral stiffness of the end towers on the responses of the bridge. The responses investigated were:

1. the sequencing of the in-plane and out-of-plane modes
2. the stress ratio in the arch ribs
3. the deck and tower lateral displacements
4. the lateral load proportioning between the arch ribs and the end towers
5. the seismic stresses compared to the wind stresses.

The study was carried out using a computer program that had been developed previously and was modified to include several measures to improve the accuracy of the analysis as well as to allow ease in the handling and gathering of the output results. The modifications include the following: a.) a new nonlinear curved beam element is used to replace the old one; b.) the dual coordinate systems is replaced by a single Cartesian system; c.) straight beams with general global geometry are allowed; d.) the two separate inputs for computer solutions (dead load - static, and then seismic - dynamic) are combined into one computer run; e.) the eigensolution needed for the specification of the Rayleigh damping is incorporated directly into the analysis (previously, this was done separately); f.) as a consequence of e.) above, the size of the time increment used in the numerical integration is made a fraction of the computed fundamental period (instead of a preset constant).; and, g.) a number of convenient measures are added for engineering studies (such as this one), they include the automatic generation of input data such as mass and stiffness quantities based on the input (dimensionless) parameters as well as the "post processing" of output data such as searching for the maximum of the response values.

The bridge model consists of two ribs as the main elements of the arch. The end towers are the "bents" at the ends of the bridge that rise from the arch support level to support the deck (Figure 1).

The major parameter in this study is α, the ratio of the lateral stiffness of the end tower to that of the rib system. The stiffness of the rib system is calculated using $F = kz$. A uniformly distributed load (F) in the Z-direction is applied to the deck and ribs and the corresponding crown displacement (z) is computed. The stiffness (k) is computed as the total load, F, divided by the displacement. The lateral stiffness of the end tower is defined as the load applied at the top of the end tower in the Z-direction to cause a unit displacement thereat.

Other parameters included in this study: span length; I_{yb}/I_{yr} (in which I_{yb} is the moment of inertia about the y-axis of the cross beam and I_{yr} is the moment of inertia about the y-axis for the rib); A_b/A_r (in which A_b is the cross sectional area of the cross beams and A_r is the cross sectional area of the rib); and, A_x/A_r (in which A_x is the cross sectional area of the rib cross-bracing). The ground motion input used in this study is that of the 1940 El Centro earthquake, with all three orthogonal components.

Three bridge span lengths are considered in this study, 200, 600 and 1000 ft. The study began with the determination of the parameter values for the bracing system between the ribs. Using eigenanalysis, the study of the inter-rib bracing parameter, I_{yb}/I_{yr}, focused on the behavior of the out-of-plane natural frequency. $I_{yb}/I_{yr} = 0.05$ was considered to be the "optimal" value to use. Similarly, the parameter A_b/A_r was set equal to 0.1. The value of A_x/A_r was set equal to 0.04 because further increase in its value would not significantly change the forces in the cross-bracing members.

The parameter α influences the eigensolutions of the arch bridge. As α is varied for a given span length, the sequencing of the in-plane and out-of-plane normal modes changes

(Table 3). An increase in end tower lateral stiffness (i.e. an increase in α) moves the in-plane modes up in ranking and the out-of-plane modes down in ranking. For relatively large values of α, the fundamental mode is an in-plane mode for span length = 200 ft. and 600 ft.; for span length = 1000 ft., it would remain to be an out-of-plane mode. For small values of α, the fundamental mode is an in-plane mode for span length = 200 ft. only; for span lengths = 600 ft. and 1000 ft., it is an out-of-plane mode.

The maximum stress ratio, SR, varies with span length and α. For span length = 200 ft., the SR varies approximately 18% from minimum to maximum. For span length = 600 ft. and 1000 ft., the SR varies approximately 5%. Therefore, for medium to long spans (i.e. 600 ft. - 1000 ft.), the SR does not vary significantly with α (Figs. 13, 14 and 15).

The effects of α on the Z-displacement, D_z, of the deck is studied. For span length = 200 ft., a reduction of 50% for D_z at the ends and middle of the deck occurs when α is increased from 0 to 0.1. For a span length = 600 ft., a 50% reduction of D_z occurs at the ends of the deck when α increases from 0 to 0.5. For the same range of α, D_z increased about 15% at the middle of the deck (Figure 22). For span length = 1000 ft., a 50% reduction of D_z at the ends of the deck occurs when α increases from 0 to 0.5. The D_z at the middle of the span increased approximately 18% when α changed from 0 to 0.1 and then decreased when α increased beyond 0.1. Among all cases, the largest D_z at the end of the deck and the middle of the deck occurred when span length = 200 ft. and α = 0. Therefore, in order to have a 50% reduction of the displacements at zero tower lateral stiffness, the shortest span, 200 ft., needs the smallest value of α.

The maximum value of the ratio of the maximum tower z-displacement to the maximum arch crown z-displacement, D_{tr}, is a function of α. For the span lengths = 600 ft. and 1000 ft., D_{tr} drops rapidly as α is increased. The span length = 200 ft. has a smoother decrease of D_{tr} as α is increased. A possible reason for the sharp decrease of D_{tr} for increasing span lengths is due to the fact that with the same width, the shorter bridge has a larger "depth-to-span ratio" with respect to the lateral loading than the longer bridge. The larger "depth-to-span ratio" represents a stiffer bridge; the larger stiffness does not allow the change in displacement to occur rapidly.

The ratio of force in the z-direction (z-force) transferred by a single tower to the z-force transferred by the rib system, α_F, is influenced by α. For each span length case , α_F is linearly related to α for small values of α. But as α increases, α_F does not remain linearly related; instead, for span lengths = 600 ft. and 1000 ft., α_F levels-off quickly, while α_F for span length = 200 ft. does not level-off as quickly. Also, the magnitude of α_F decreases as span length increases; in other words, the amount of force transferred to the towers decreases with increasing span length (Figure 29).

For the three span lengths, a comparison of stresses due to wind load and seismic loads was made. It is shown that for the span length = 200 ft., the seismic stress dominates for all values of α. For span length = 1000 ft., the wind stress is larger than the seismic stress. But for span length = 600 ft. and small values of α (less than or equal to 0.1), the wind stress is larger than the seismic stress; for larger α, the seismic stress becomes larger than the wind stress. It is observed that for longer spans, the wind stress would govern; seismic stress governs for short spans.

4.2 Conclusion

A study of the seismic behavior of the deck-type arch bridges in the three dimensional space has been conducted. In the study, emphasis has been placed on the role of the end towers of the bridge systems when the structure is subjected to a ground motion that has a lateral component. It is found that the behavior is governed mainly by the parameter α, the ratio of the tower lateral stiffness to that of the rib system.

As α varies, the lateral or out-of-plane natural frequencies change, and the seismic response changes accordingly. It is found that such changes had a larger effect for bridges with a short span length (200 ft.) than the longer ones (600 ft. or 1000 ft.). When compared with the usual strength requirement, or in terms of stresses, the results obtained indicated for shorter spans, the lateral design load would be based on the seismic load rather than the wind load. For longer spans, the wind load would be the governing lateral design load.

For displacement, generally, the larger the α, for any span length, the less the displacement of the deck and ribs.

Based on the results obtained, there seems to be not a need for a large value of α; a value of 0.5 or 1.0 may be sufficient.

The seismic stresses presented here could be scaled. The scaling factor may be based on the seismic response coefficient, C_s. According to AASHTO Bridge Seismic Specification, C_s can be calculated as $C_s = 1.2*Ac*S/T^{2/3}$
where Ac = the ground acceleration coefficient; S = the dimensionless coefficient for the soil profile characteristics of the site; and T = the period of the bridge. If one takes A = 0.4 and S = 1 for the El Centro earthquake and the dynamic analysis used, the scaling factor, SF_{site}, would simply be the seismic response coefficient of the new site to the seismic response coefficient corresponding to the El Centro earthquake, i.e. $SF_{site} = (AS)_{site}/(AS)_{El\ Centro}$ or, $SF_{site} = (AS)_{site}/0.4$. The seismic stresses presented herein may then be multiplied by SF_{site} to obtain the stresses that may occur at the site.

It is recognized that the data presented herein covered only a very small part of the range of parameters. In a specific design situation, it would be necessary to obtain a computer solution based on the parameter values of the structure being planned. But the results presented here should provide insight into the behavior of such bridges and aid the engineer in the preliminary stages of the design, particularly with reference to the design of the end tower.

Future research along the line of the study here may consider such "secondary" parameters, for example, I_{xr}/I_{yr}, the moment of inertia about the x-axis of the rib to the moment of inertia about y-axis of the rib. Also, different earthquake motions (real and artificial) might be used in the future to develop a more general description of the bridge behavior. Cost studies could be implemented to study the cost-benefit relation for lateral stiffness of the end towers.

TABLES

Table 1 Parameters for In-Plane and Additional Parameters for Out-of-Plane Studies.

Parameters for In-Plane Behavior	Range	Value Used
H/L	0.125 - 0.225	0.175
L/r_y	100, 300	200
G	2.63 - 10.5	10.5
M_r/M	0.344 - 0.760	0.265
N	6 - 24	8
ξ	2%, 5%	2%
c_y/r_y	1.00 - 1.55	1.27
L	200 - 1000 ft.	200, 600, 1000
x_g	0 - 0.50g	0.31g
y_g	0 - 0.50g	0.23g
Additional Parameters for Out-of-Plane Behavior		
W	30 - 60	30
I_{xr}/I_{yr}	0.32 - 0.11	0.32 - 0.11
c_x/r_x	1.00 - 1.55	1.30
A_x/A_r	Not Available	0.04
A_b/A_r	0.10 - 0.25	0.10
I_{yb}/I_{yr}	0.0015 - 0.014	0.05
I_{xb}/I_{yb}	Not Available	1.0
K_{tb}/I_{yb}	Not Available	1.0
α	0.0 - 10.0	0 - 10
A_s/A_r	Not Available	0.183 - 0.91
z_g	0 - 0.50g	0.31g

Table 2 Distribution of Stresses vs. Loading in Curved Beams ($L = 600'$, $\alpha = 1.0$).

Member	Case	Stress	SAM	SYM	SXM
1 (9)	x-only	4.72	1.0	0.0	0.0
	y-only	1.83	1.0	0.0	0.0
	z-only	8.78	0.65	0.0	0.35
2 (10)	x-only	25.25	0.03	0.97	0.0
	y-only	3.01	0.57	0.43	0.0
	z-only	11.77	0.23	0.66	0.11
3 (11)	x-only	36.16	0.02	0.98	0.0
	y-only	3.85	0.42	0.58	0.0
	z-only	3.99	0.03	0.70	0.27
4 (12)	x-only	31.36	0.03	0.97	0.0
	y-only	4.36	0.36	0.64	0.0
	z-only	5.79	0.34	0.51	0.15
5 (13)	x-only	8.75	0.98	0.01	0.0
	y-only	4.55	0.34	0.66	0.0
	z-only	12.6	0.15	0.70	0.15
6 (14)	x-only	25.59	0.03	0.97	0.0
	y-only	4.41	0.36	0.63	0.0
	z-only	5.09	0.02	0.74	0.23
7 (15)	x-only	42.06	0.03	0.97	0.0
	y-only	3.94	0.43	0.57	0.0
	z-only	5.83	0.45	0.35	0.20
8 (16)	x-only	40.19	0.04	0.96	0.0
	y-only	3.13	0.58	0.42	0.0
	z-only	15.19	0.37	0.52	0.11

Table 3 Natural Frequencies (cps).

α	Modes	L = 200′	L = 600′	L = 1000′
0.0	1	in 0.634	out 0.250	out 0.126
	2	out 0.811	out 0.274	out 0.133
	3	out 0.845	in 0.367	in 0.284
	4	in 1.559	out 0.767	out 0.315
	5	in 2.103	in 0.902	in 0.699
	T_{in} (s)	1.59	2.70	3.52
	T_{out} (s)	1.23	4.00	7.94
0.1	1	in 0.634	out 0.292	out 0.163
	2	out 0.901	in 0.367	out 0.194
	3	out 1.057	out 0.362	in 0.284
	4	in 1.559	out 0.802	out 0.339
	5	out 2.107	in 0.902	in 0.699
	T_{in} (s)	1.58	2.70	3.52
	T_{out} (s)	1.11	3.42	6.13
0.5	1	in 0.635	in 0.367	out 0.209
	2	out 1.169	out 0.375	in 0.284
	3	in 1.559	out 0.585	out 0.328
	4	out 1.631	in 0.902	out 0.446
	5	out 2.127	out 0.947	in 0.699
	T_{in} (s)	1.57	2.70	3.52
	T_{out} (s)	0.86	2.63	4.78
9.0	1	in 0.635	in 0.367	out 0.233
	2	in 1.559	out 0.470	in 0.284
	3	out 1.911	in 0.902	out 0.604
	4	out 2.675	out 1.287	in 0.699
	5	in 2.903	in 1.680	out 0.921
	T_{in} (s)	1.57	2.70	3.52
	T_{out} (s)	0.52	2.13	4.29

Table 4 Comparison of Wind and Seismic Stresses.

	stress	α=0.1	α=0.5	α=1.0	α=2.0	α=3.0	α=8.0
L=1000′	wind max	9.49	7.59	7.15	6.89	6.80	6.68
	seis max	1.76	1.73	1.47	1.46	1.68	1.53
	wind 1/4	5.38	4.26	4.00	3.85	3.80	3.73
	seis 1/4	2.42	2.42	2.28	2.24	2.18	2.26
L=600′	wind max	10.24	7.25	6.33	5.74	5.52	5.23
	seis max	7.55	9.51	6.88	6.75	9.22	9.25
	wind 1/4	4.20	2.85	2.43	2.16	2.06	1.93
	seis 1/4	1.87	2.77	2.19	2.44	2.44	2.26
L=200′	wind max	6.57	3.96	2.82	1.97	1.62	1.13
	seis max	17.42	20.22	21.98	28.74	28.50	17.56
	wind 1/4	3.09	1.79	1.21	0.79	0.62	0.37
	seis 1/4	7.52	9.48	11.86	13.84	14.25	9.17

FIGURES

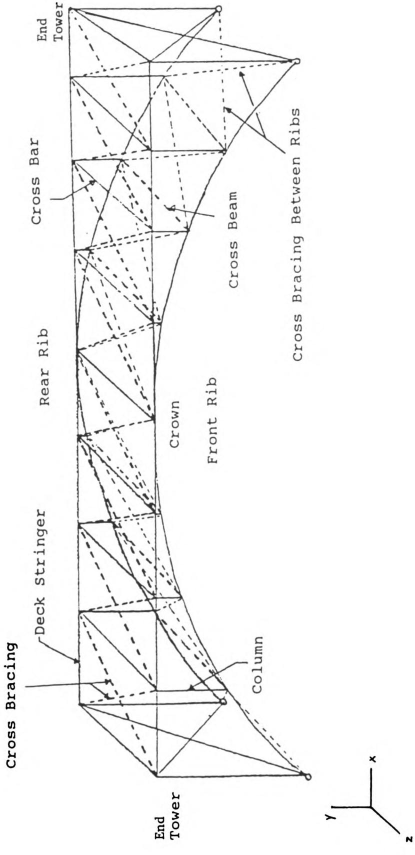

Figure 1 Sketch of Bridge Model.

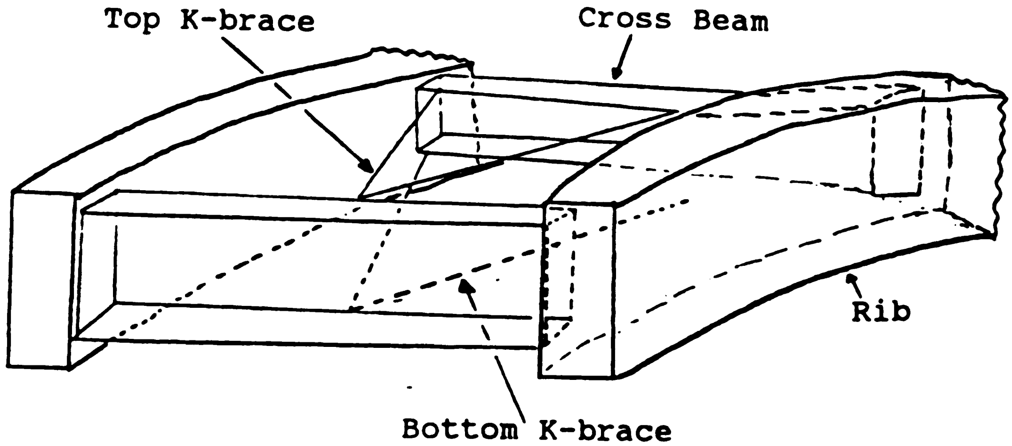

(a) Torsional Box

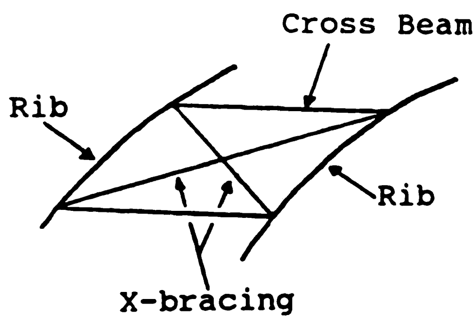

(b) Computer Model

Figure 2 Cross-section of Twin-rib System and Computer Model.

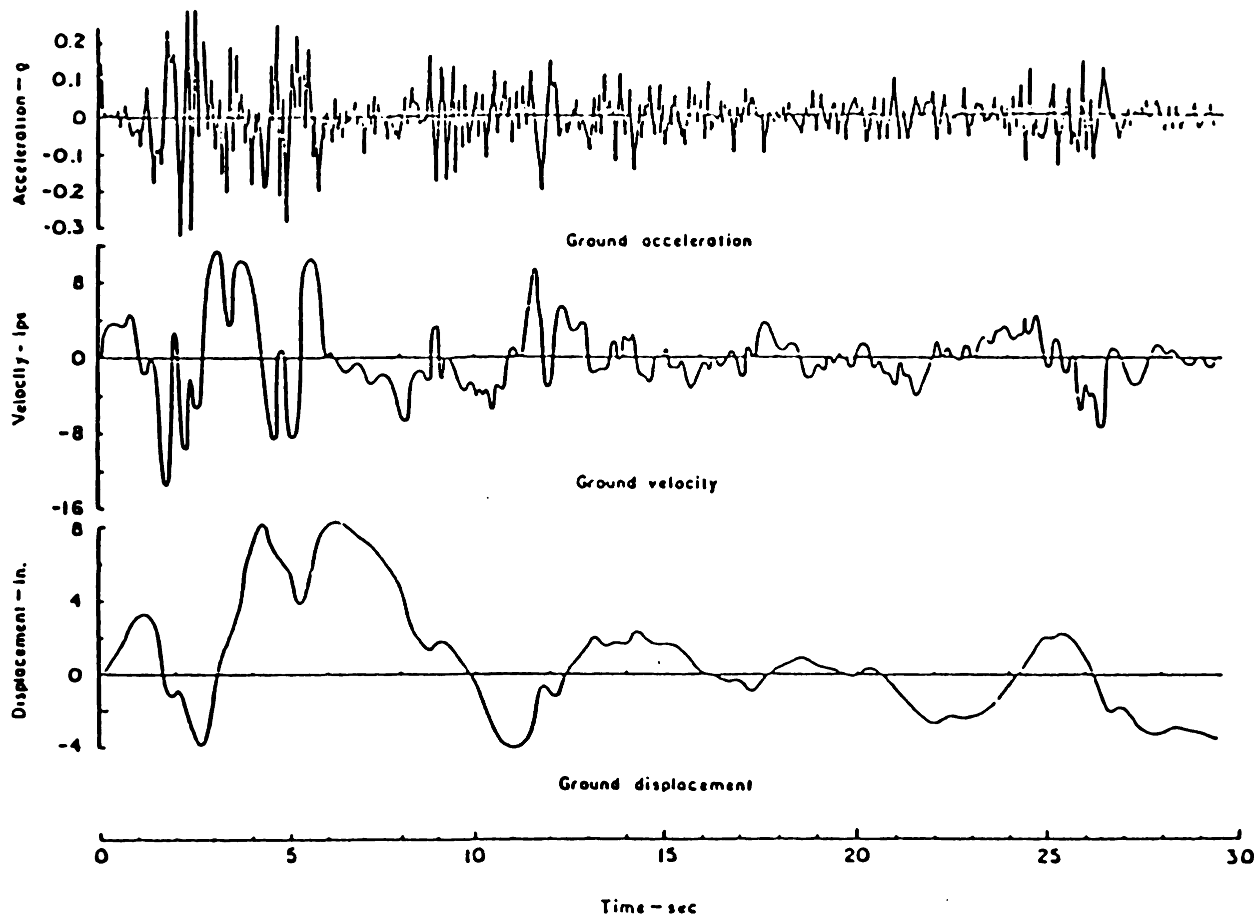

Figure 3 Ground Acceleration, Velocity and Displacement of 1940 El Centro Earthquake.

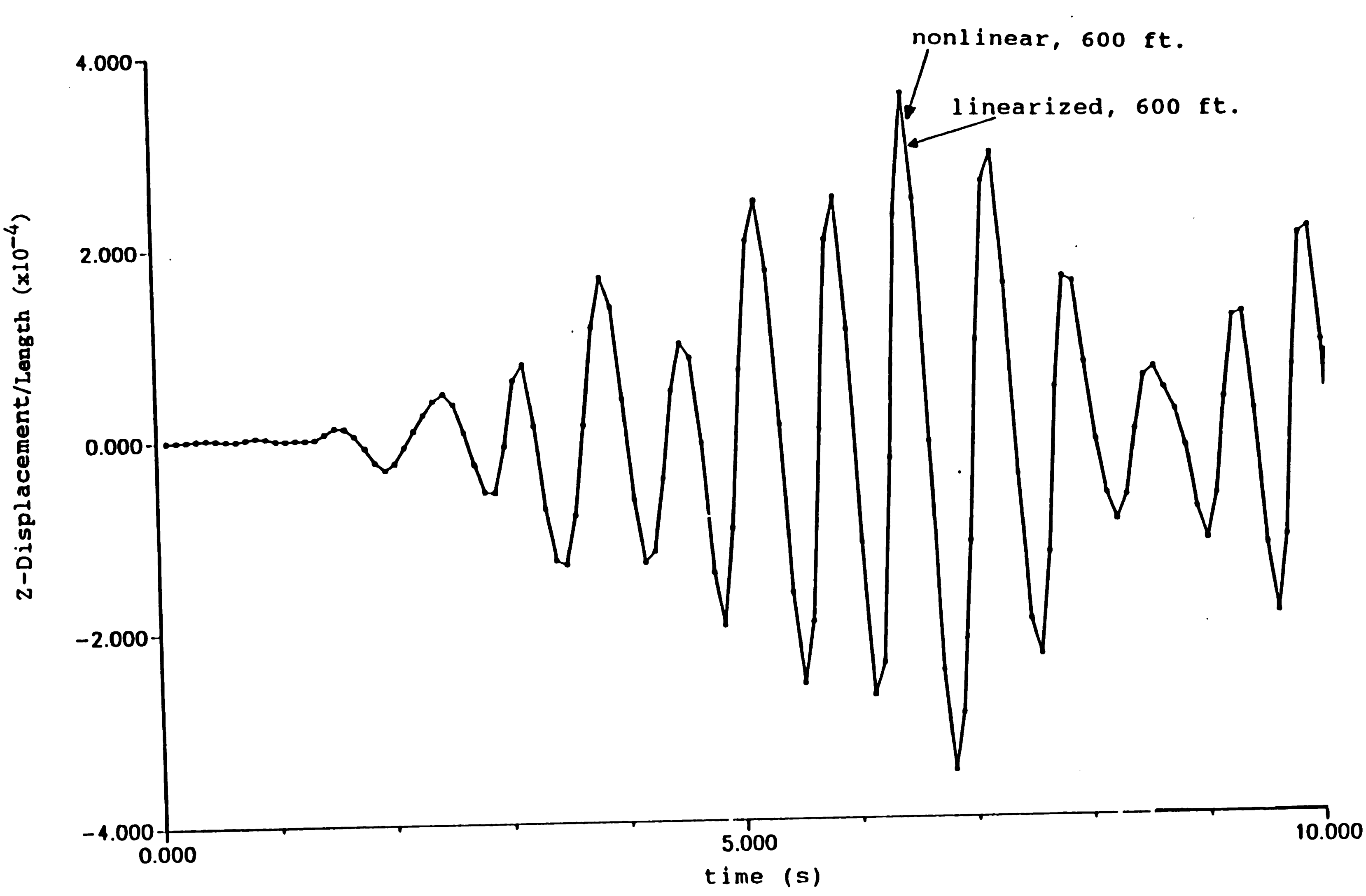

Figure 4 Z-displacement of Quarter Point as Function of Nonlinear and Linearized Analysis.

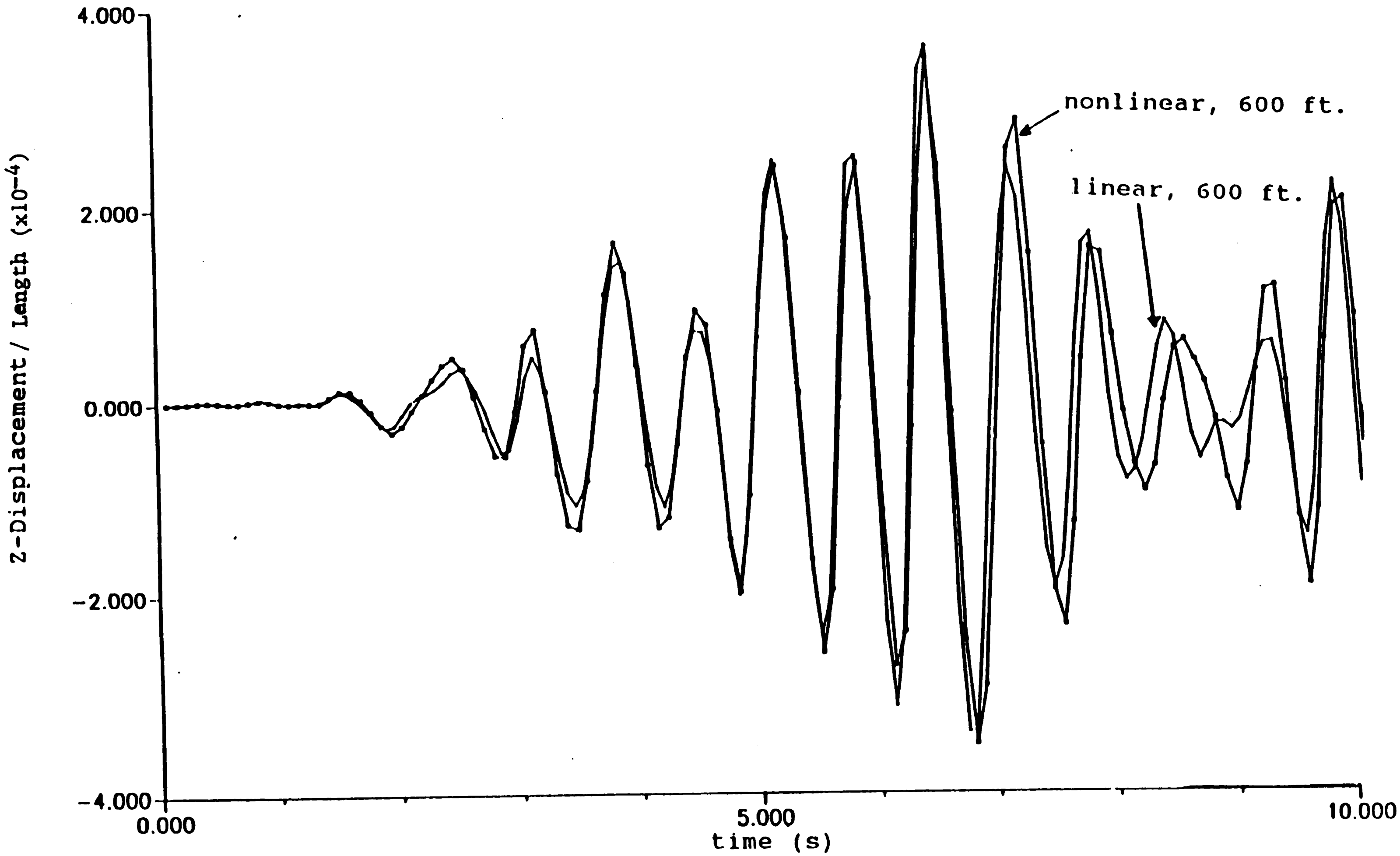

Figure 5 Z-displacement of quarter Point as a Function of Linear and Nonlinear Analysis.

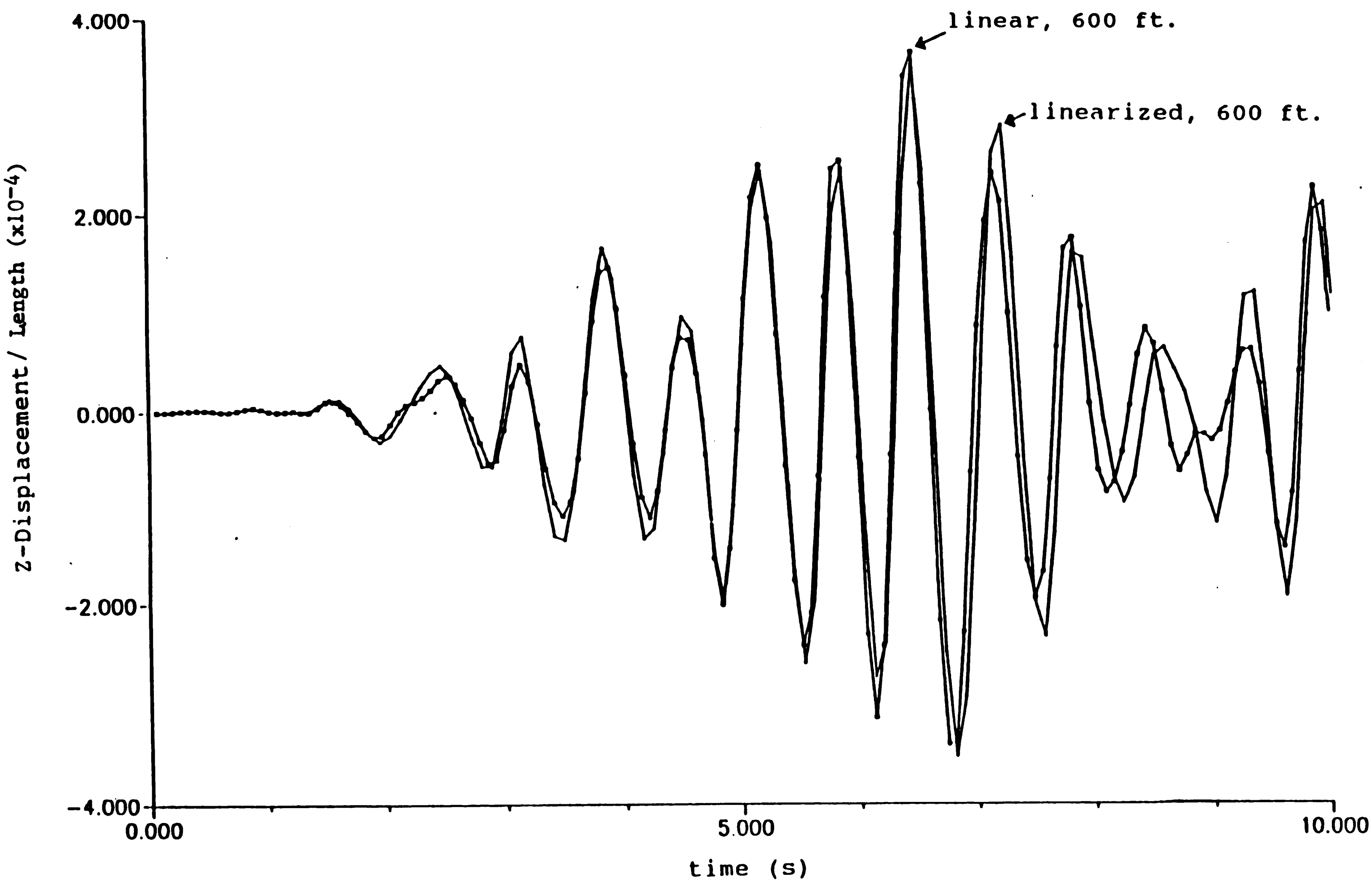

Figure 6 Z-displacement of Quarter Point as Function of Linear and Linearized Analysis.

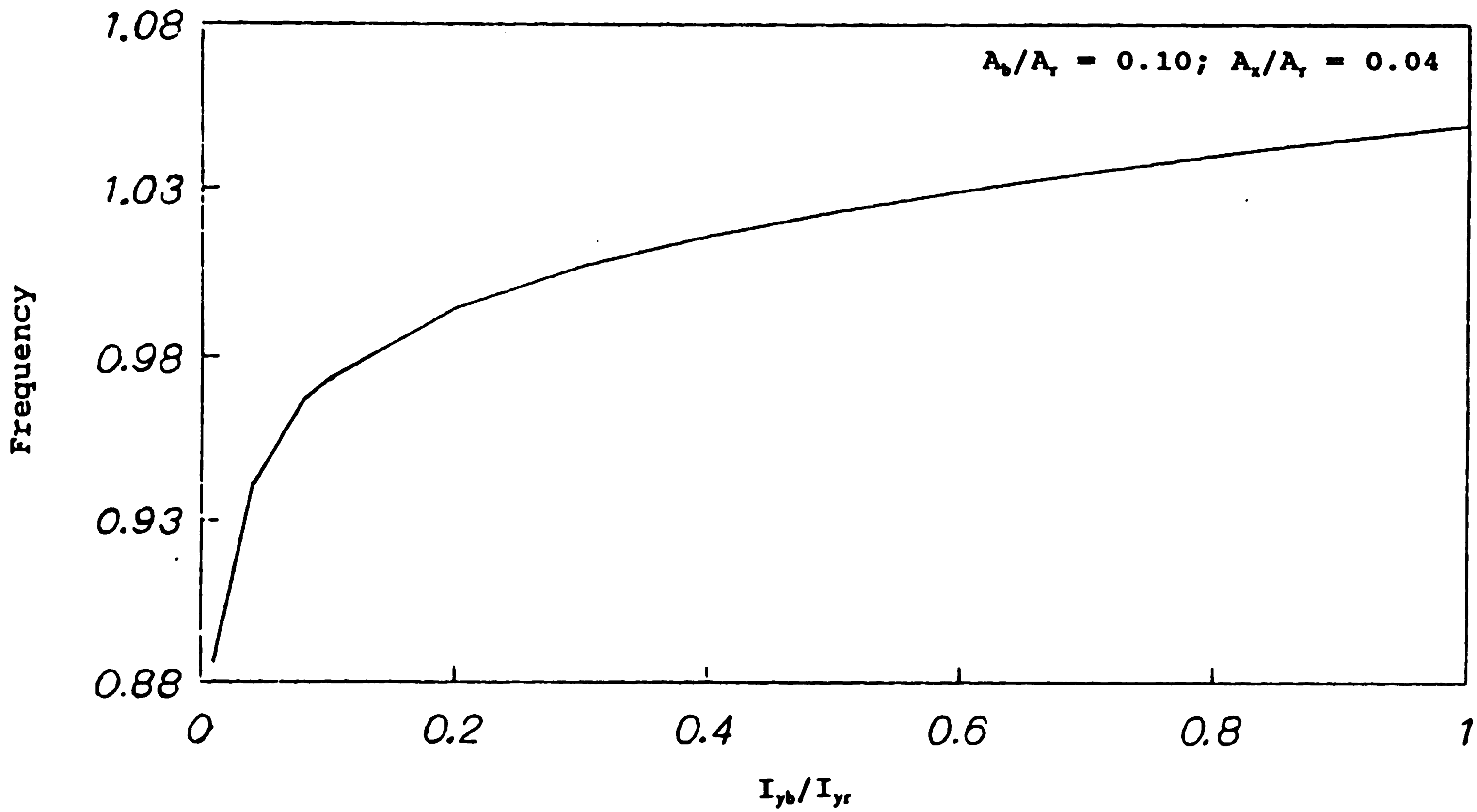

Figure 7 First Out-of-Plane Natural Frequency as a Function of I_{yb}/I_{yr}.

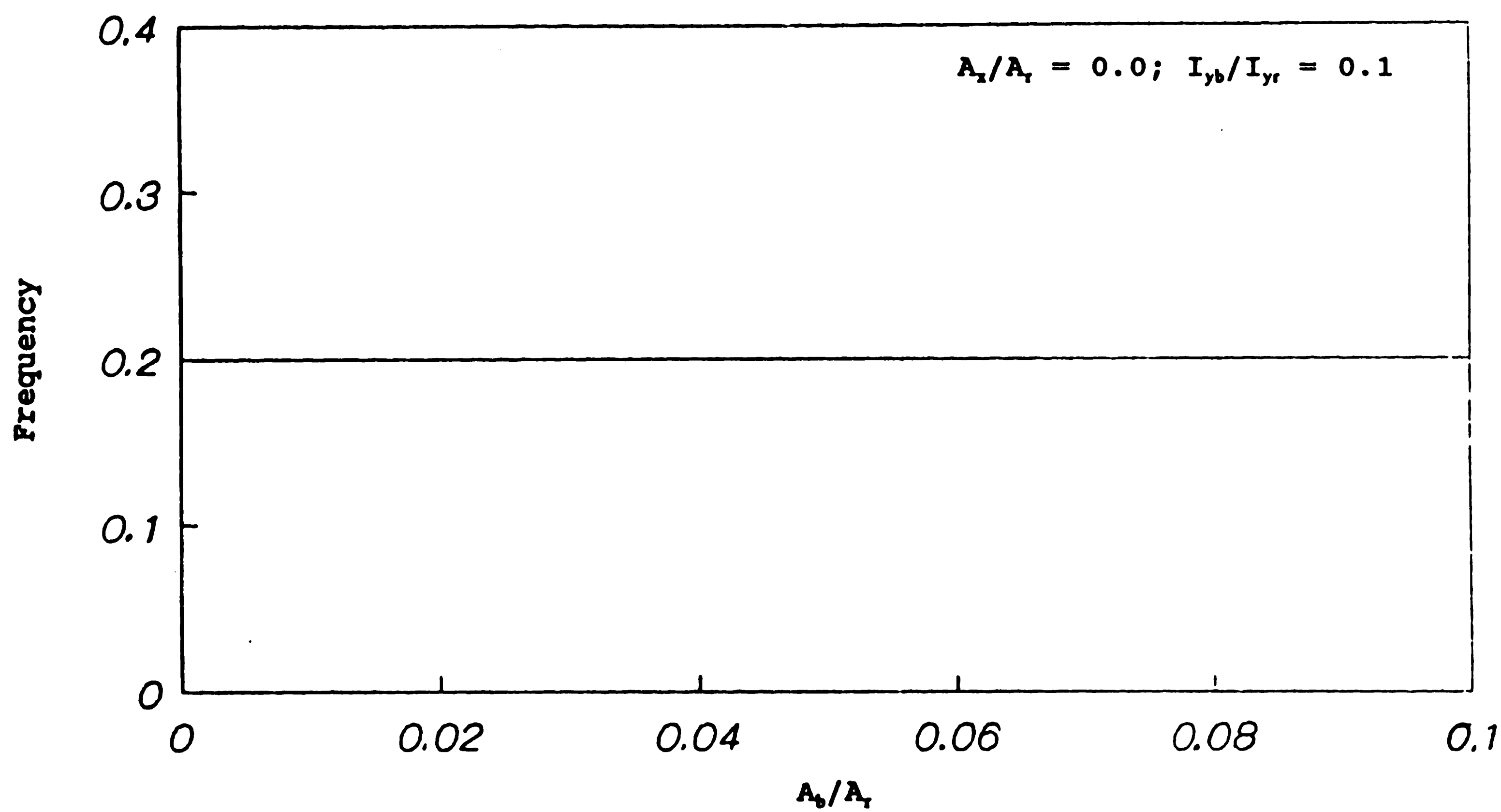

Figure 8 First Out-of-Plane Natural Frequency.

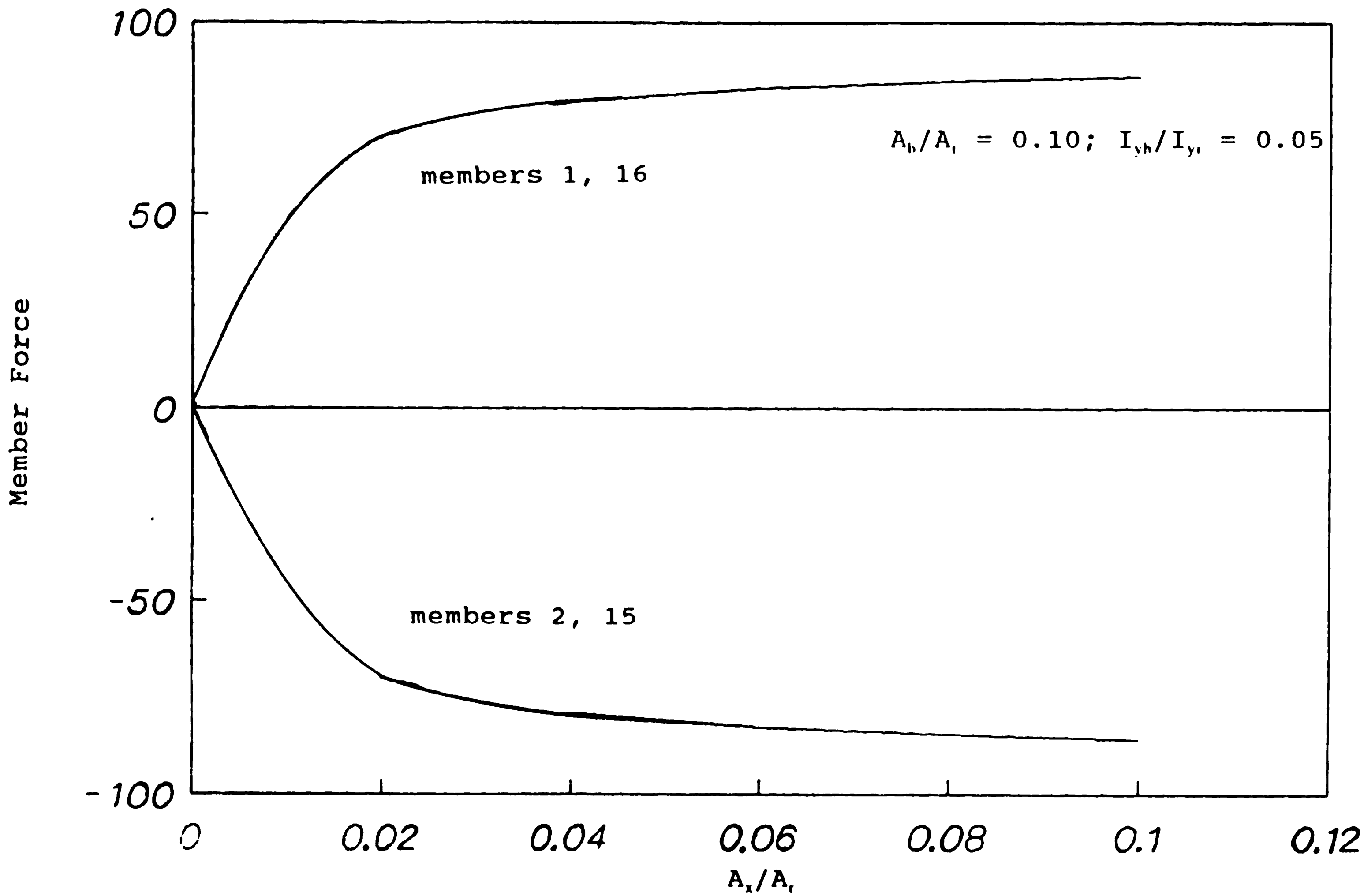

Figure 9 Rib Force Due to Static Z-load.

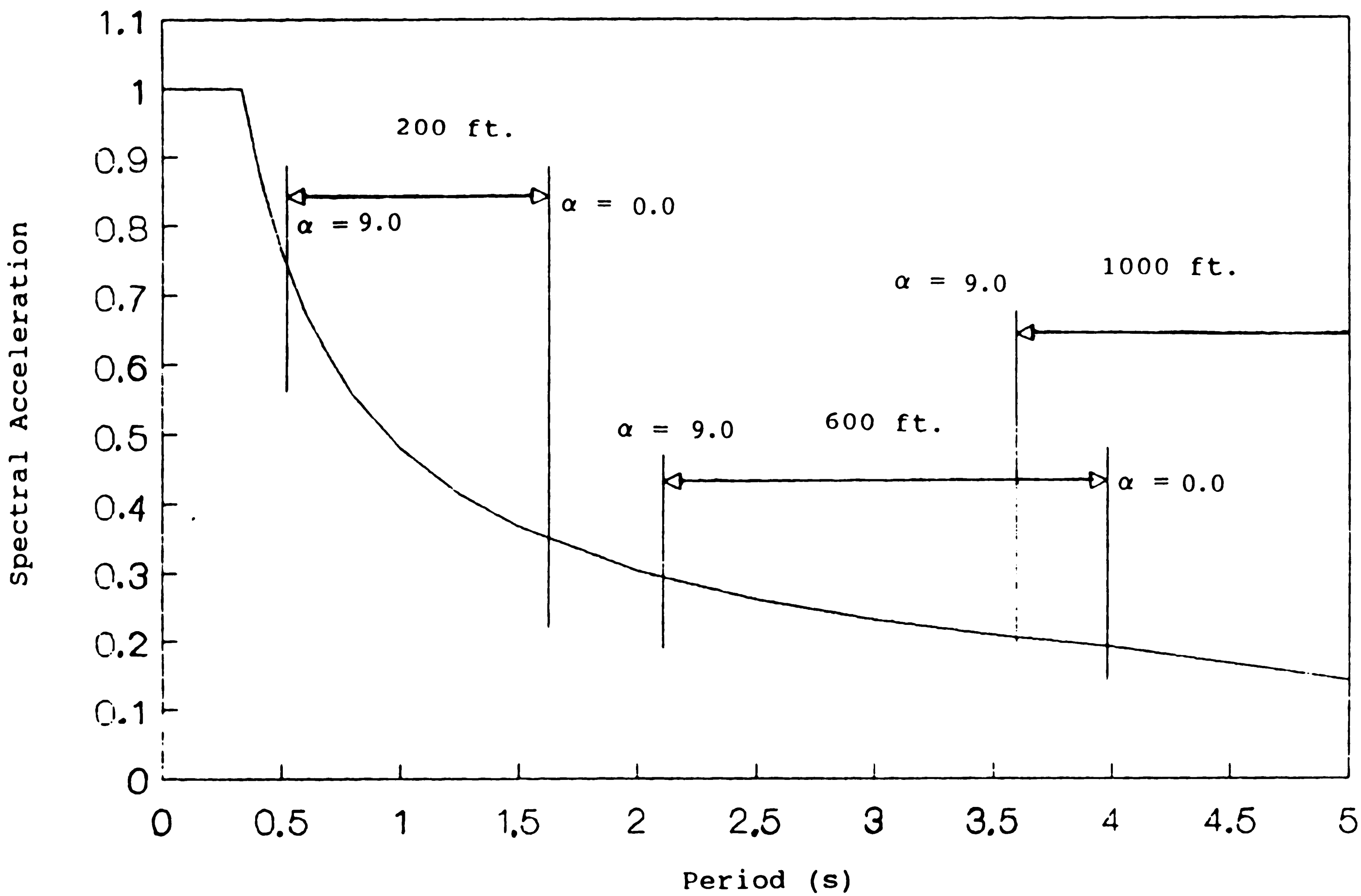

Figure 10 Response Spectrum as a Function of Period.

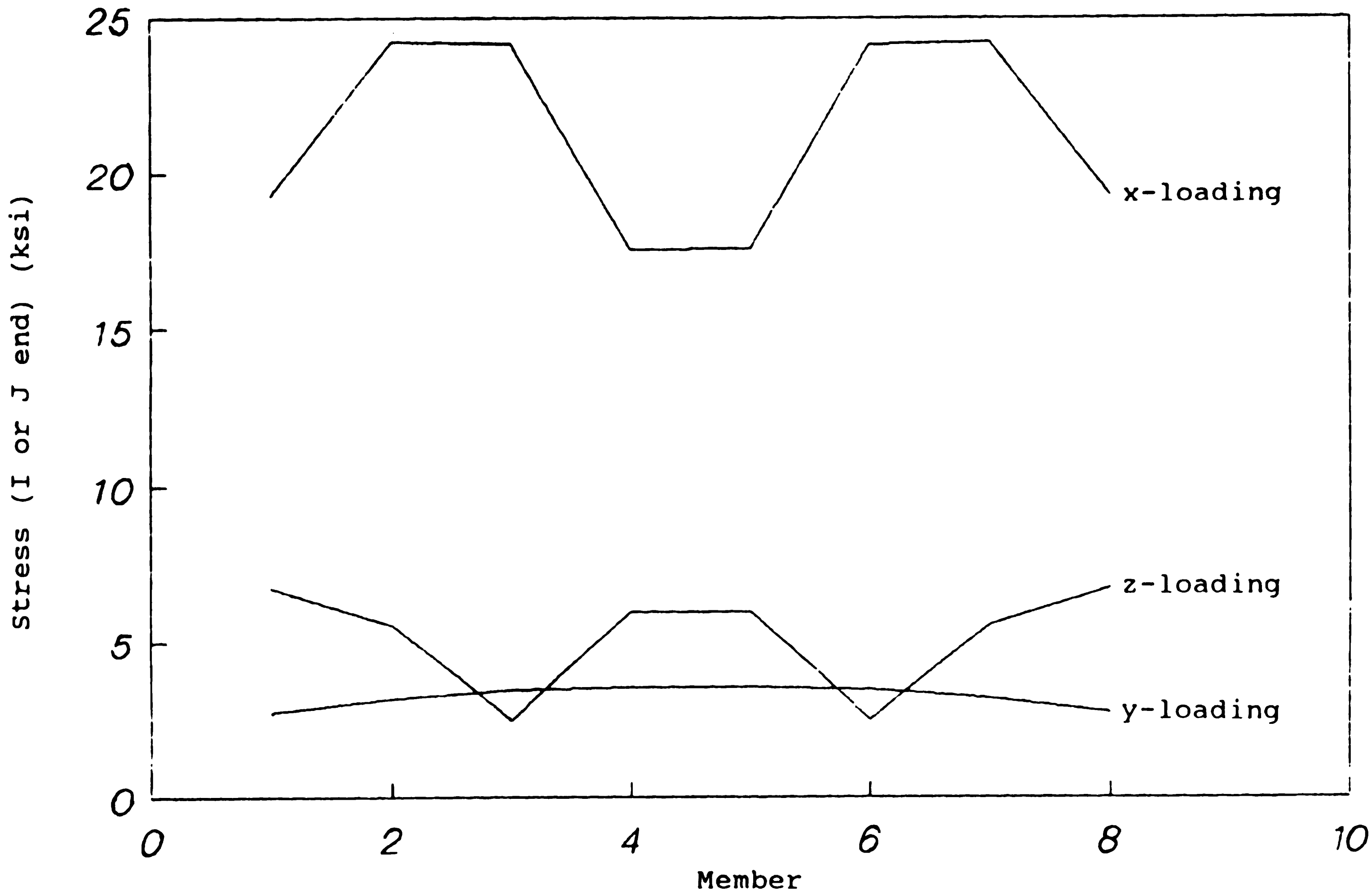

Figure 11 Distribution of Stress in a Rib (L = 200 ft.).

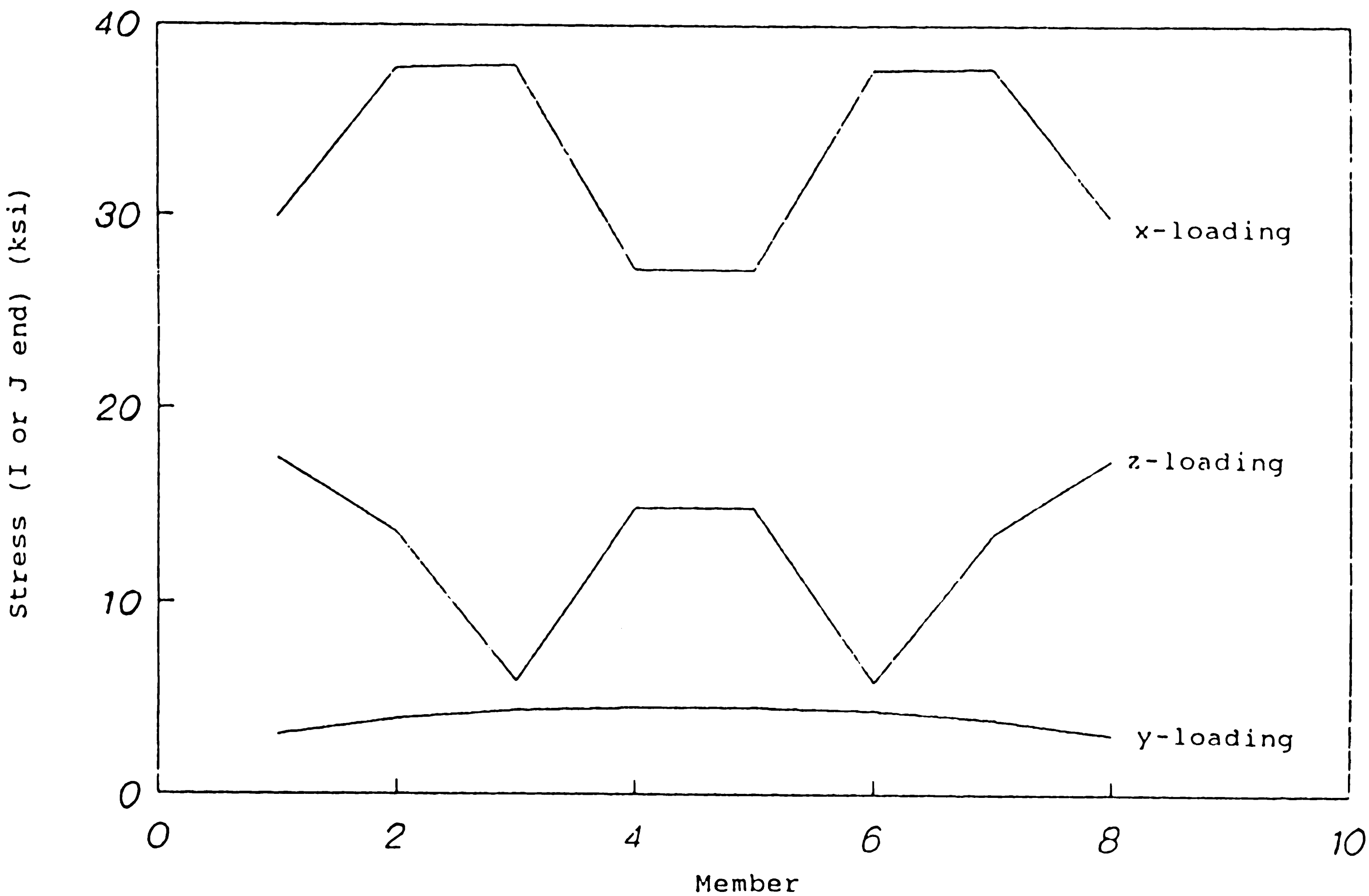

Figure 12 Distribution of Stress in a Rib (L = 600 ft.)

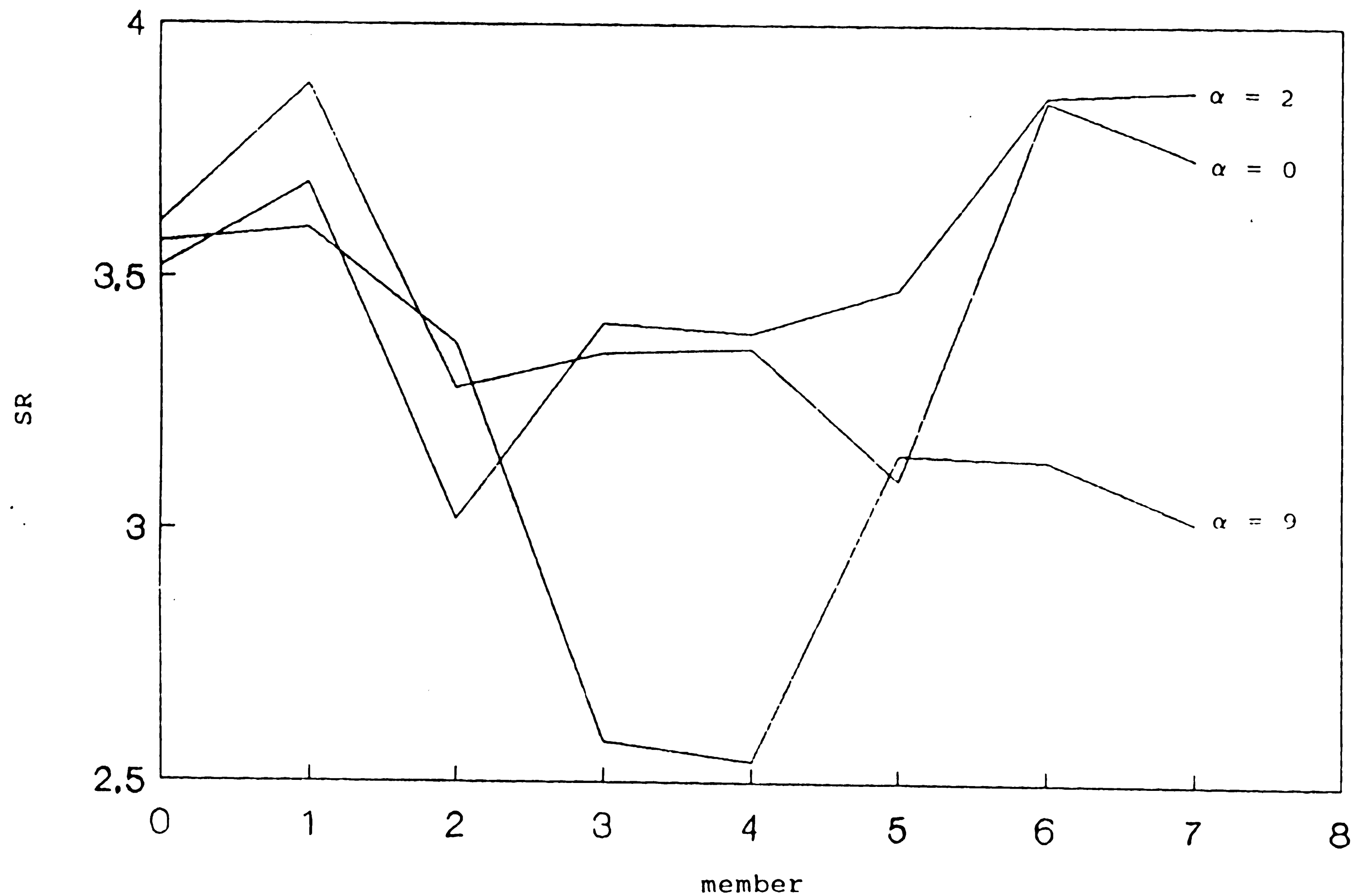

Figure 13 Distribution of SR (L = 200 ft.).

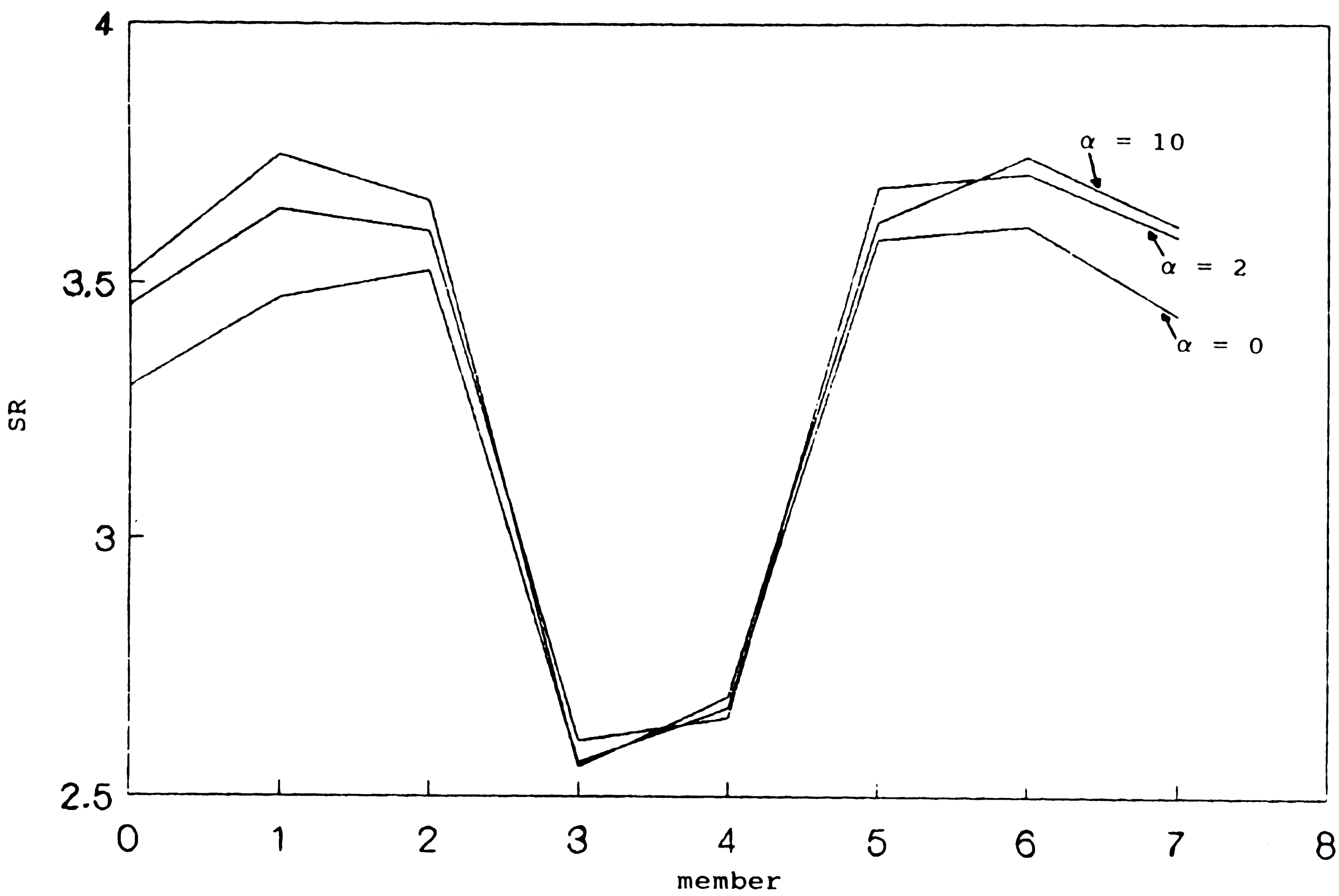

Figure 14 Distribution of SR (L = 600 ft.).

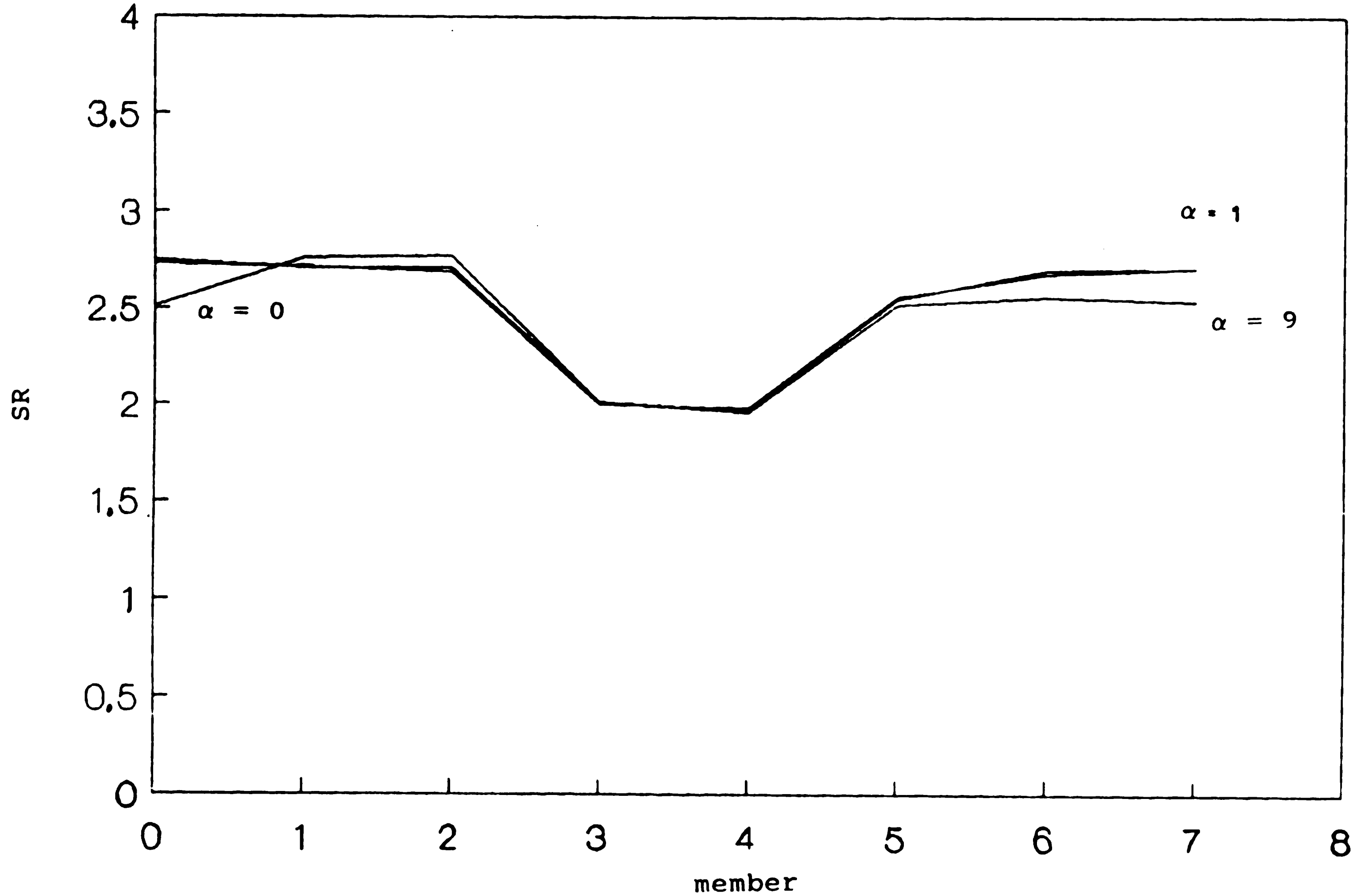

Figure 15 Distribution of SR (L = 1000 ft.).

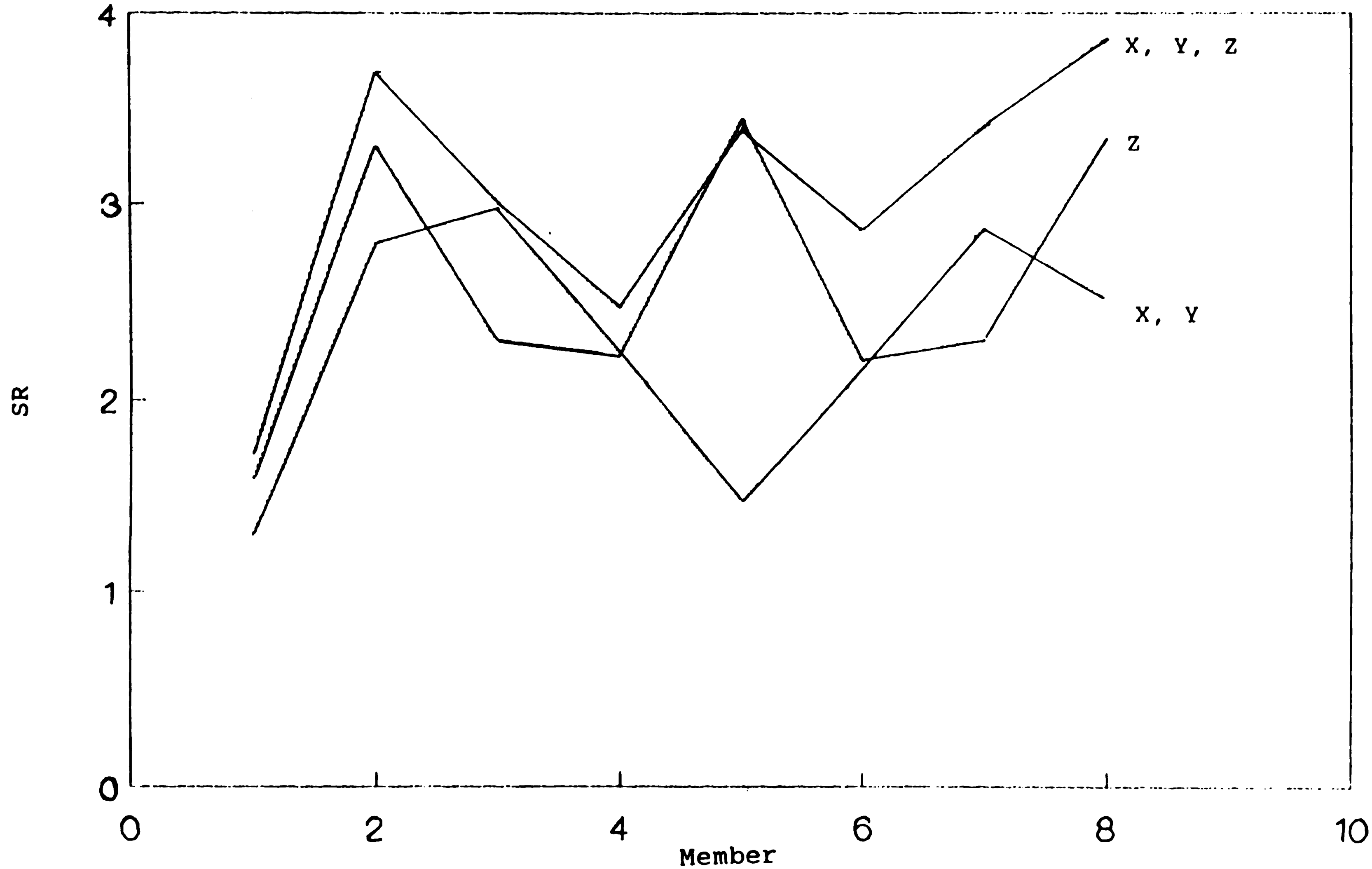

Figure 16 SR for Different Combination of Earthquake Components.(L = 200 ft.)

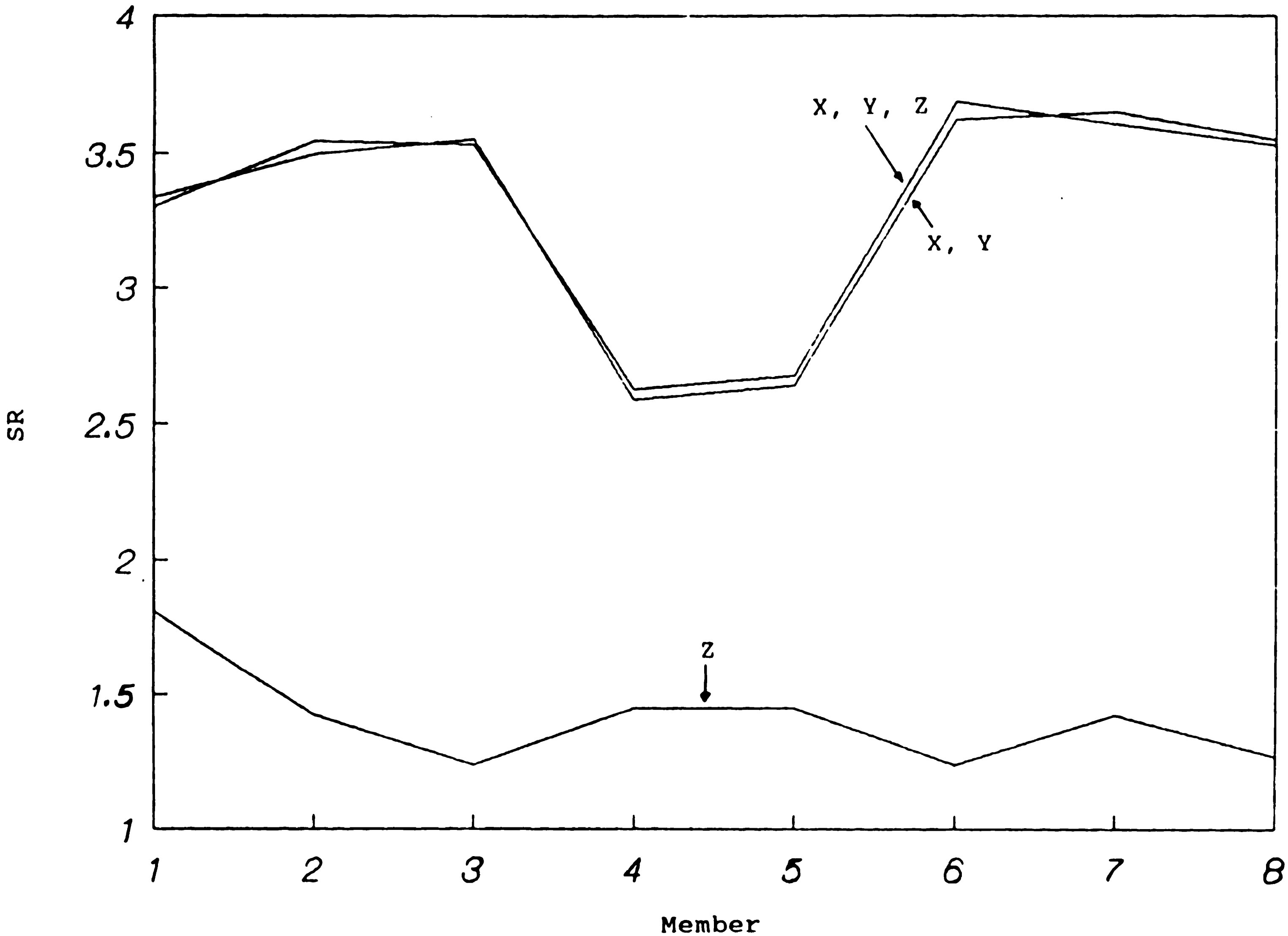

Figure 17 SR for Different Combination of Earthquake Components.(L = 600 ft.)

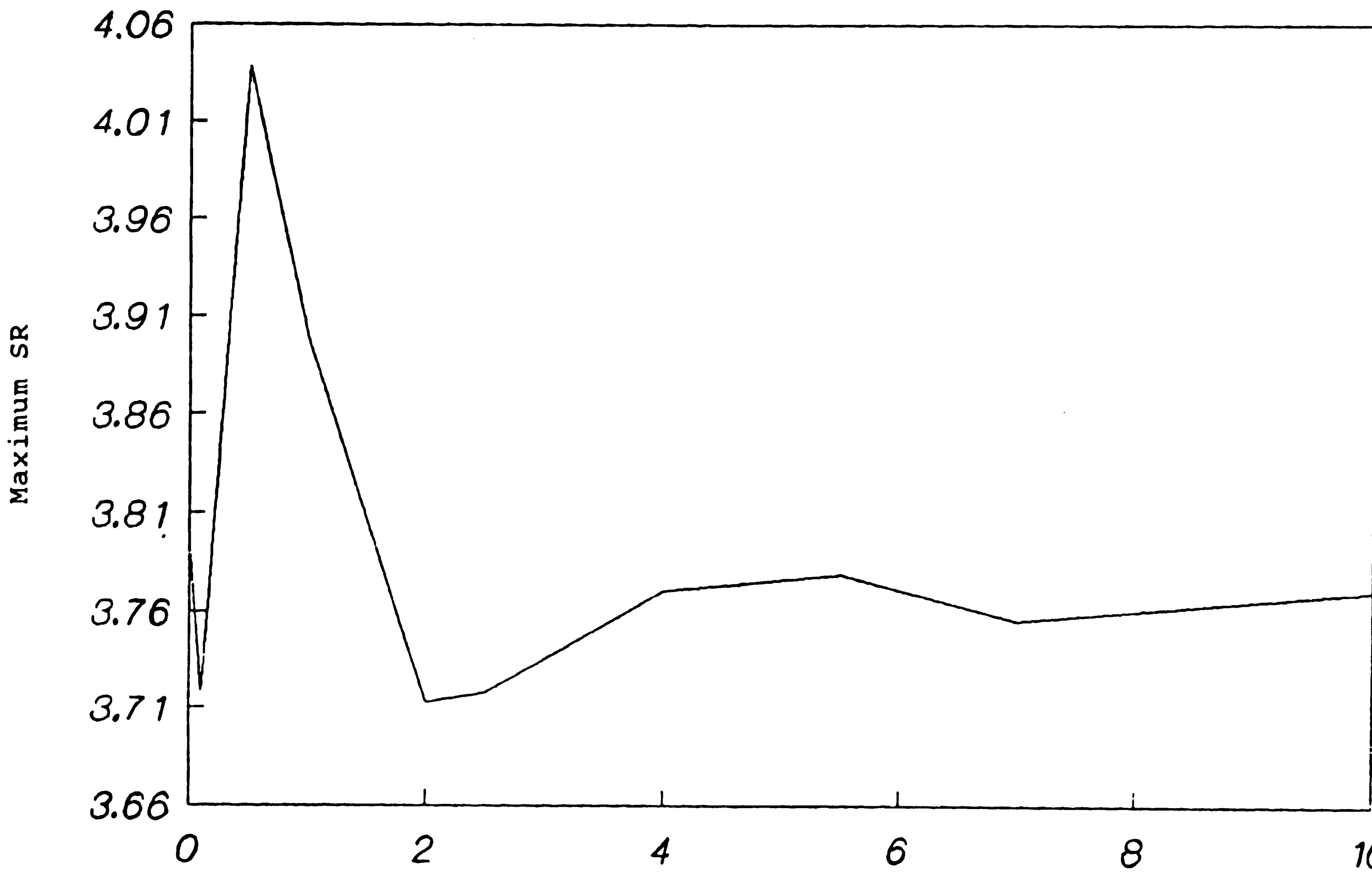

Figure 18 Maximum SR as a Function of α (L = 600 ft.).

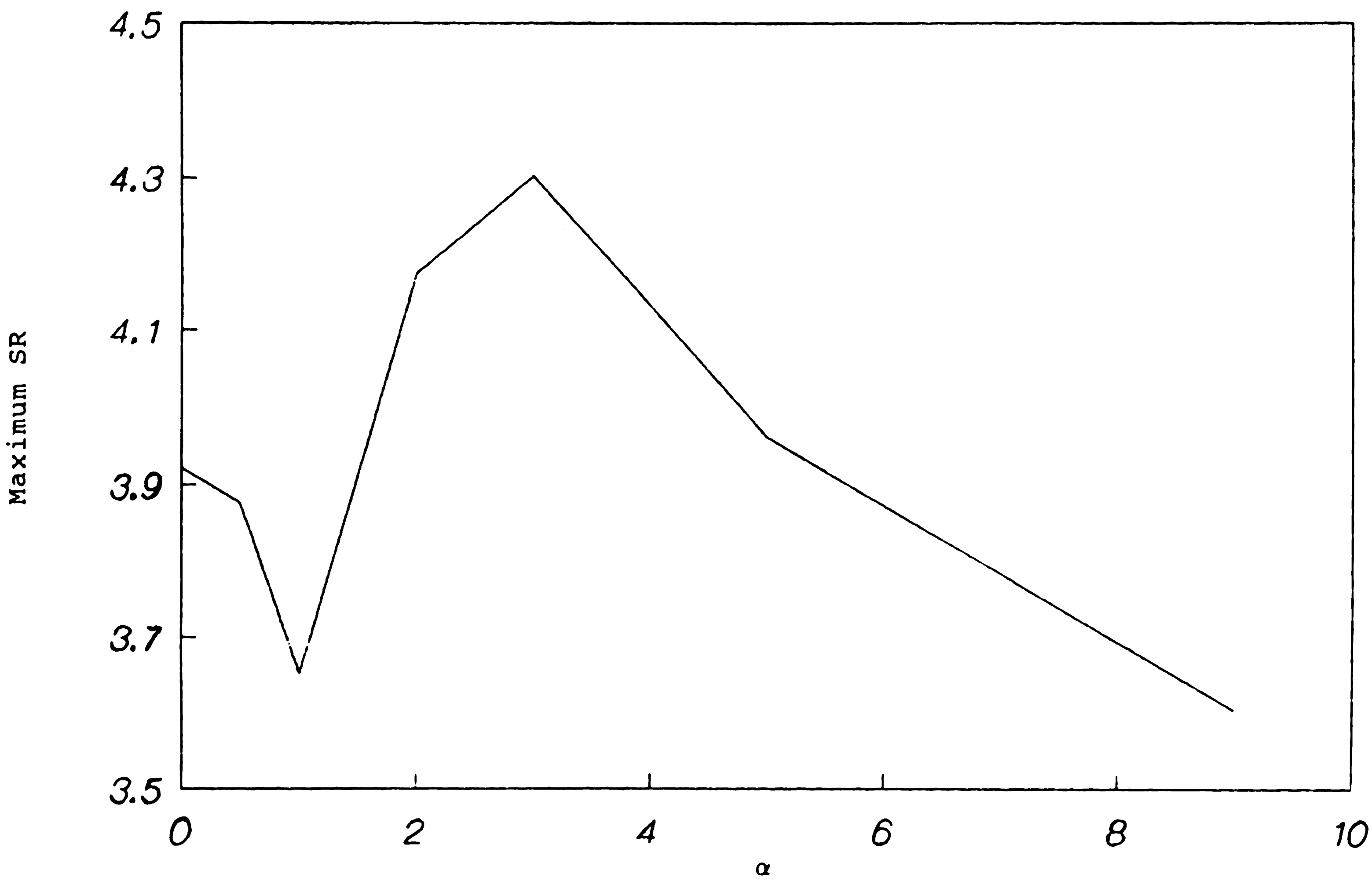

Figure 19 Maximum SR as a Function of α (L = 200 ft.).

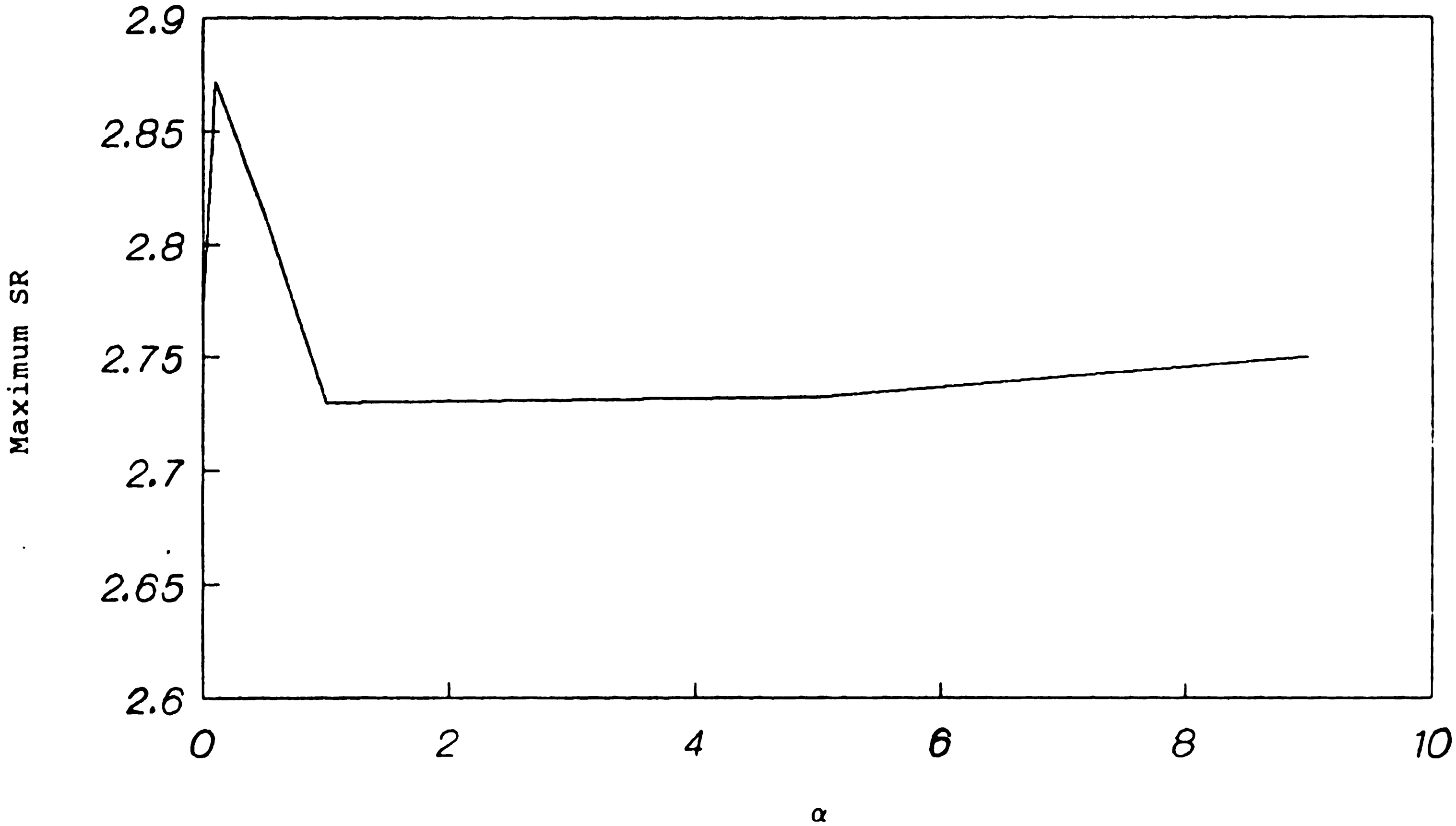

Figure 20 Maximum SR as a Function of α (L = 1000 ft.).

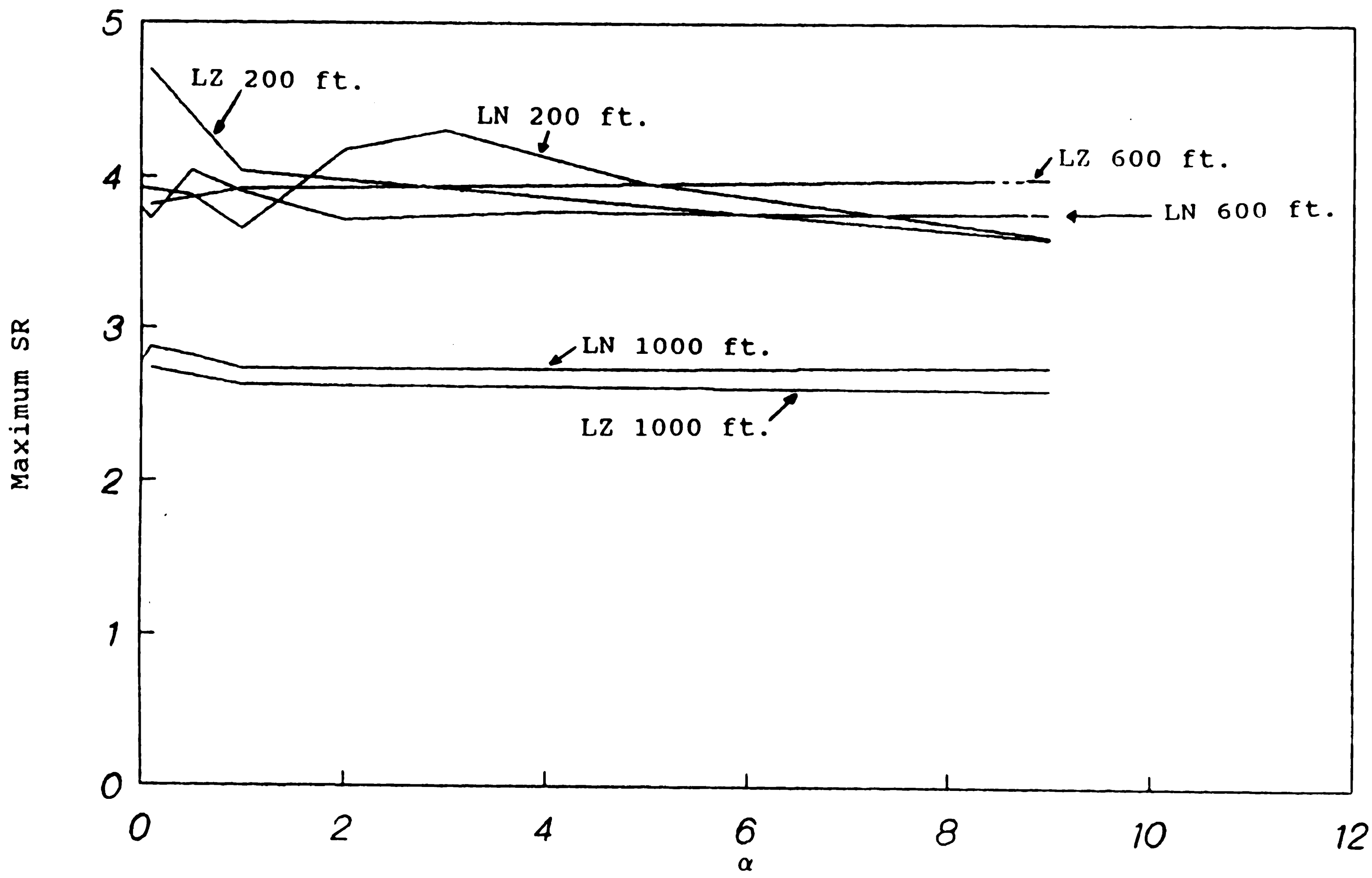

Figure 21 Linear and Linearized Analysis.

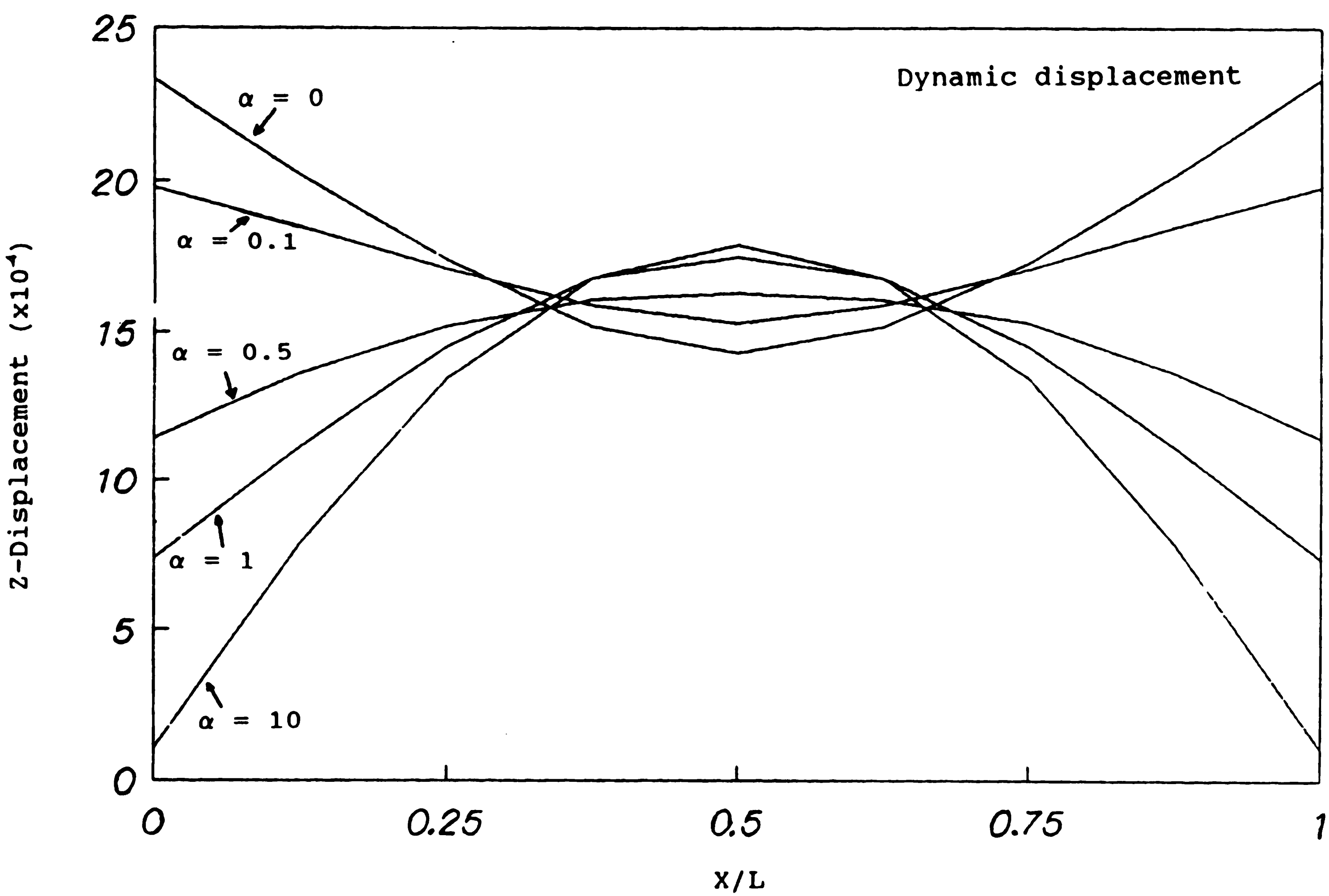

Figure 22 Deck Z-Displacement Along Span Length (L = 600 ft.).

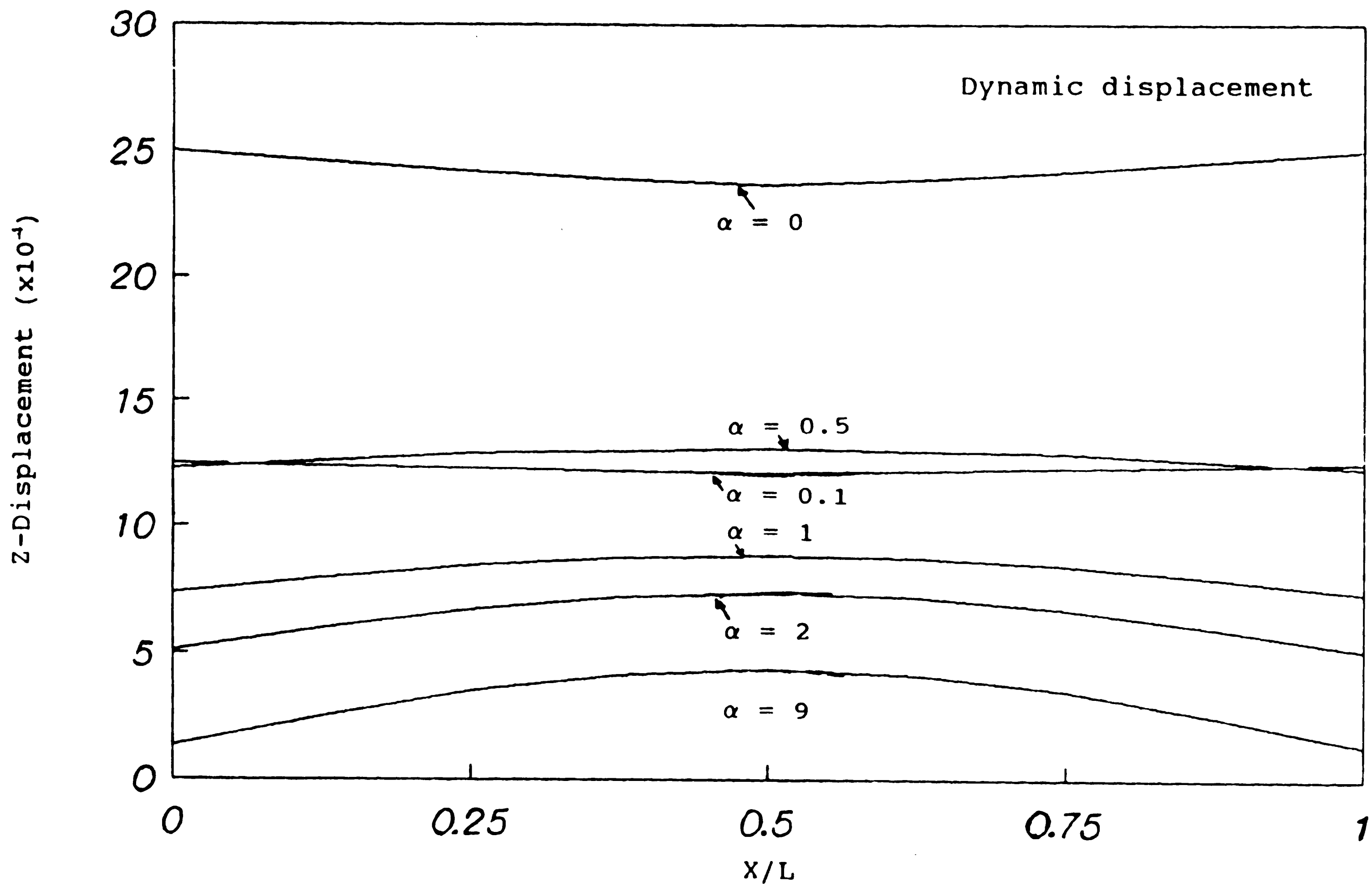

Figure 23 Deck Z-Displacement as a Function of α (L = 200 ft.).

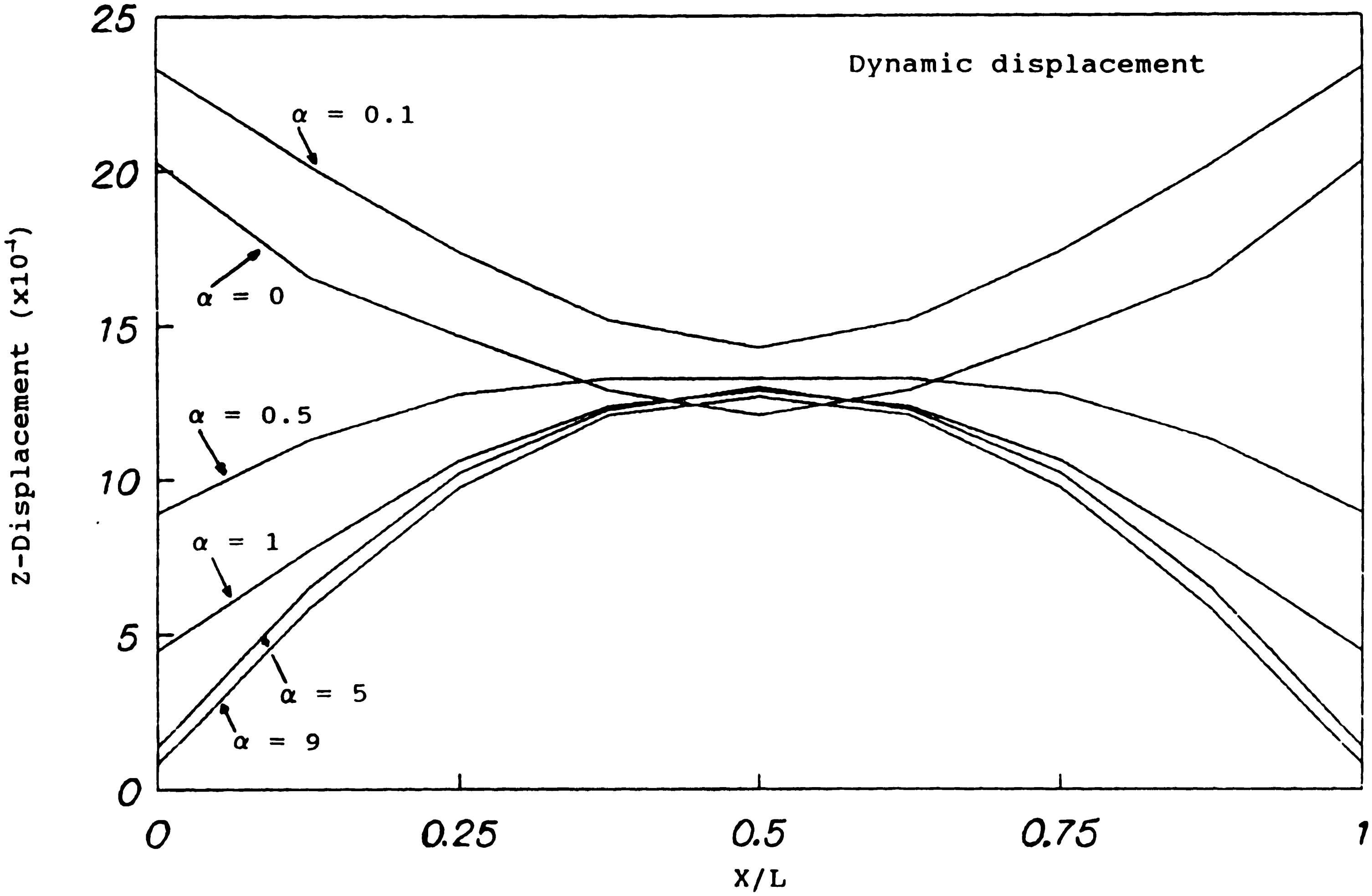

Figure 24 Deck Z-Displacement Along Span Length (L = 1000 ft.).

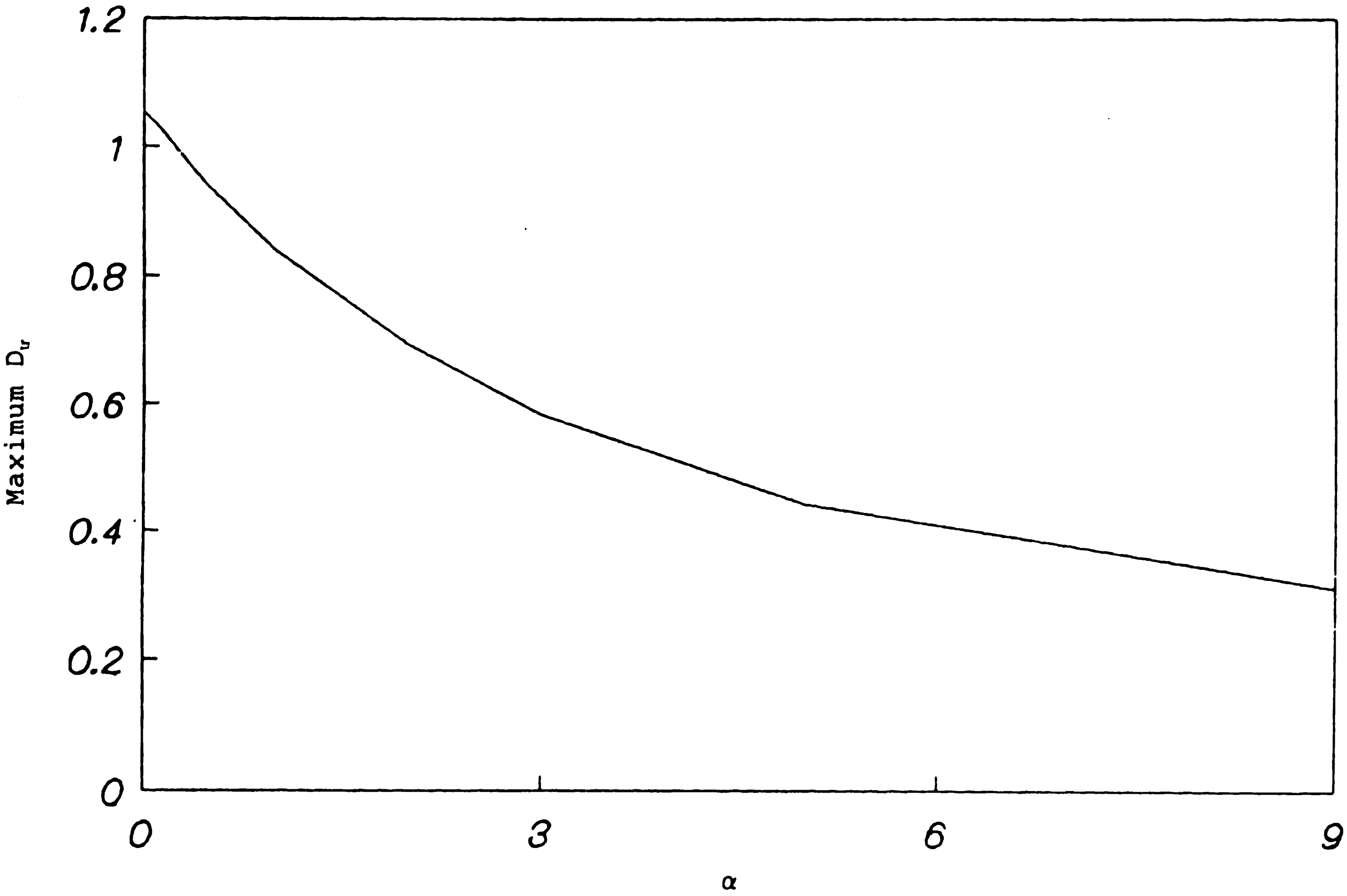

Figure 25 Maximum Tower D_{tr} as a Function of α (L = 200 ft.).

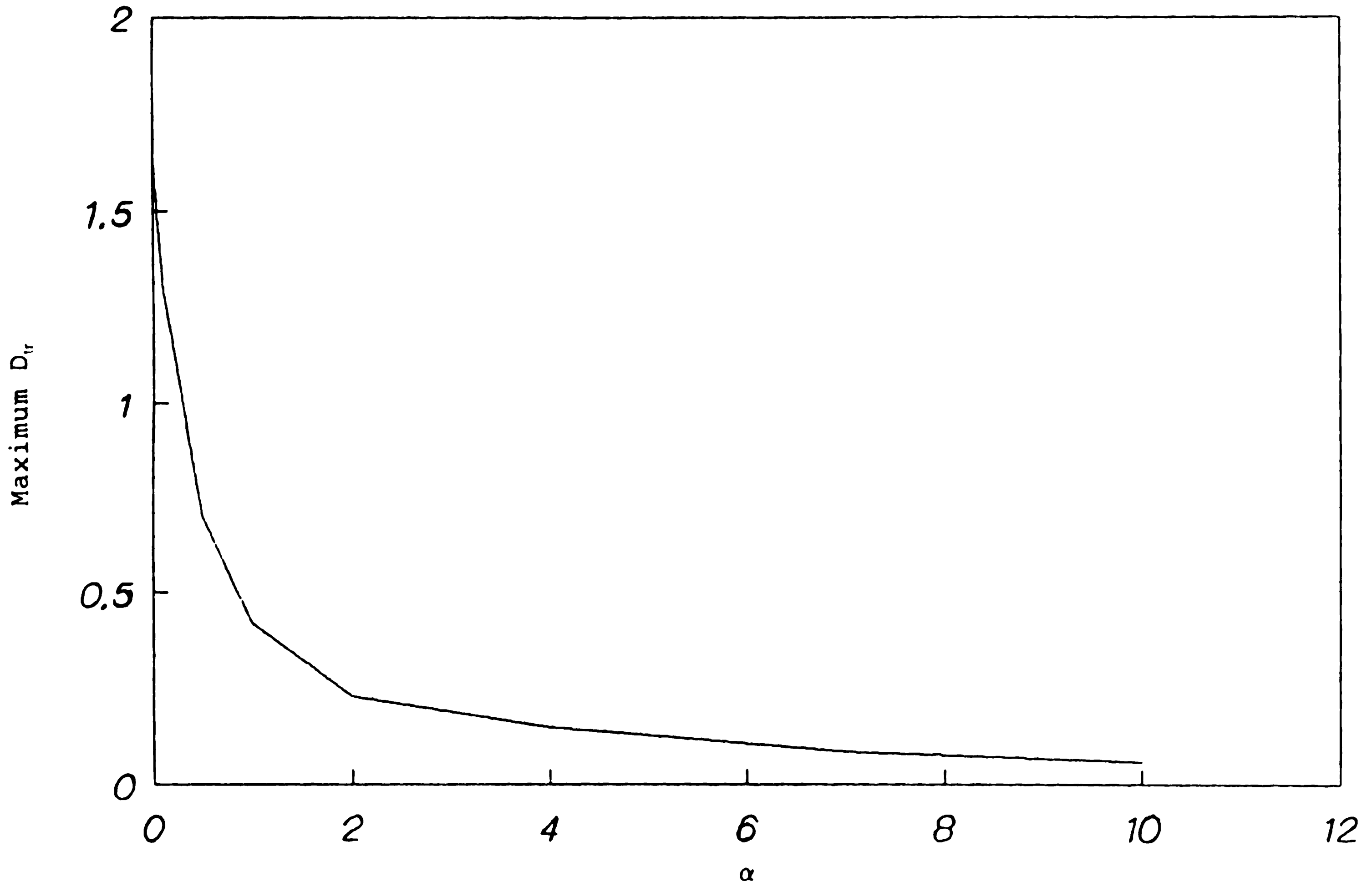

Figure 26 Maximum Tower D_{tr} as a Function of α (L = 600 ft.).

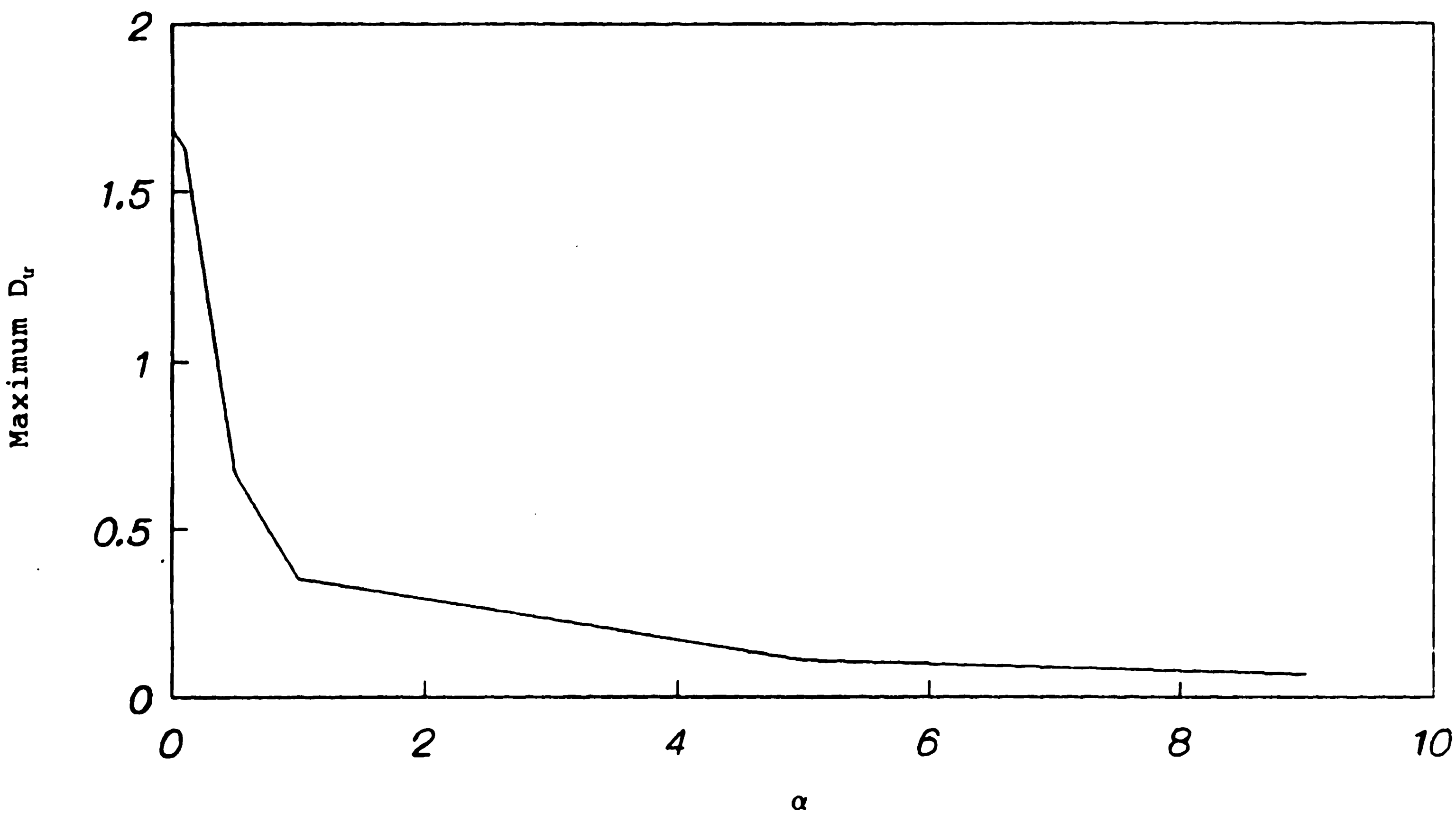

Figure 27 Maximum Tower D_{tr} as a Function of α (L = 1000 ft.).

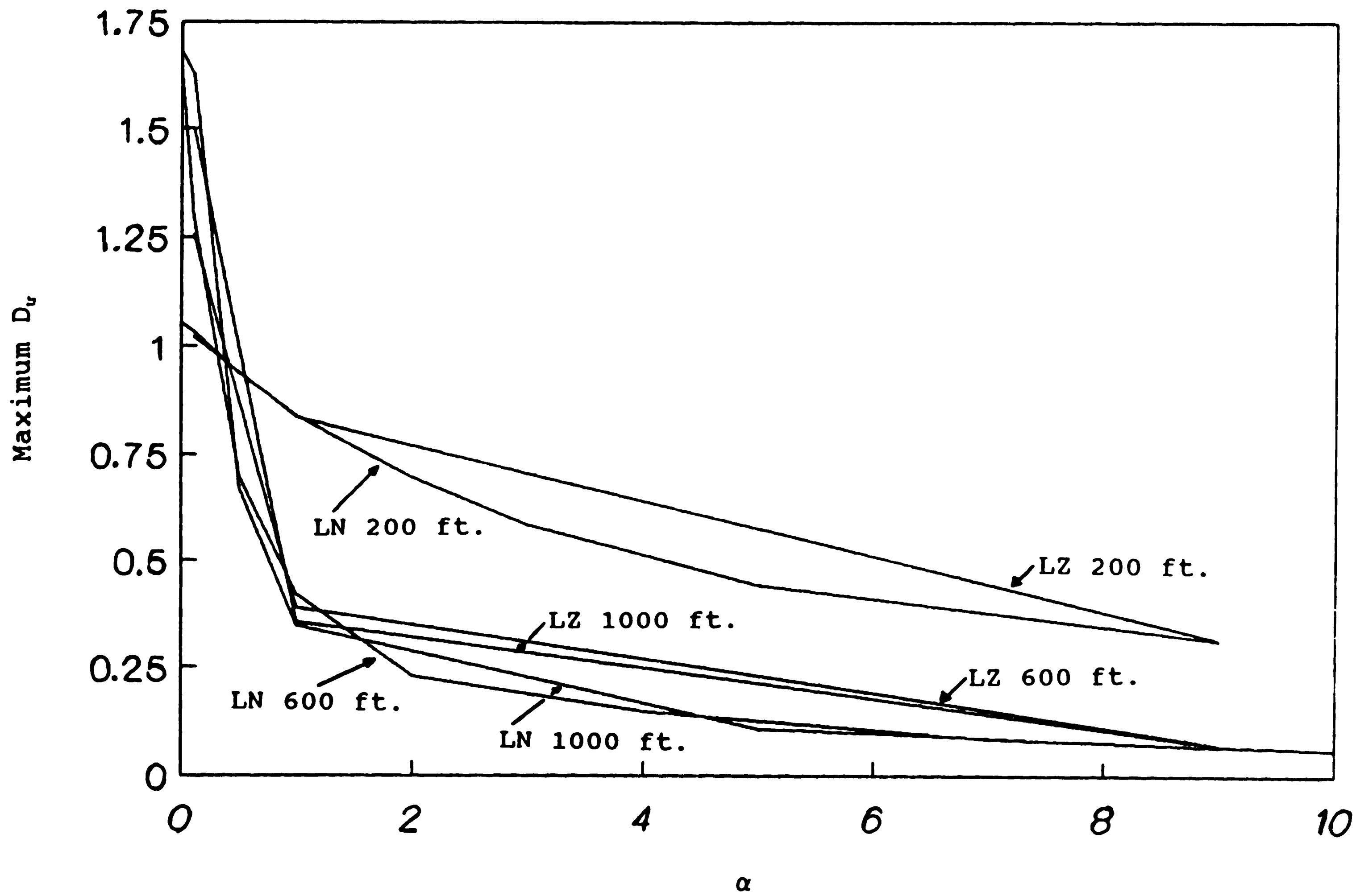

Figure 28 Linear and Linearized Analysis (L = 200 ft., 600 ft., 1000 ft.).

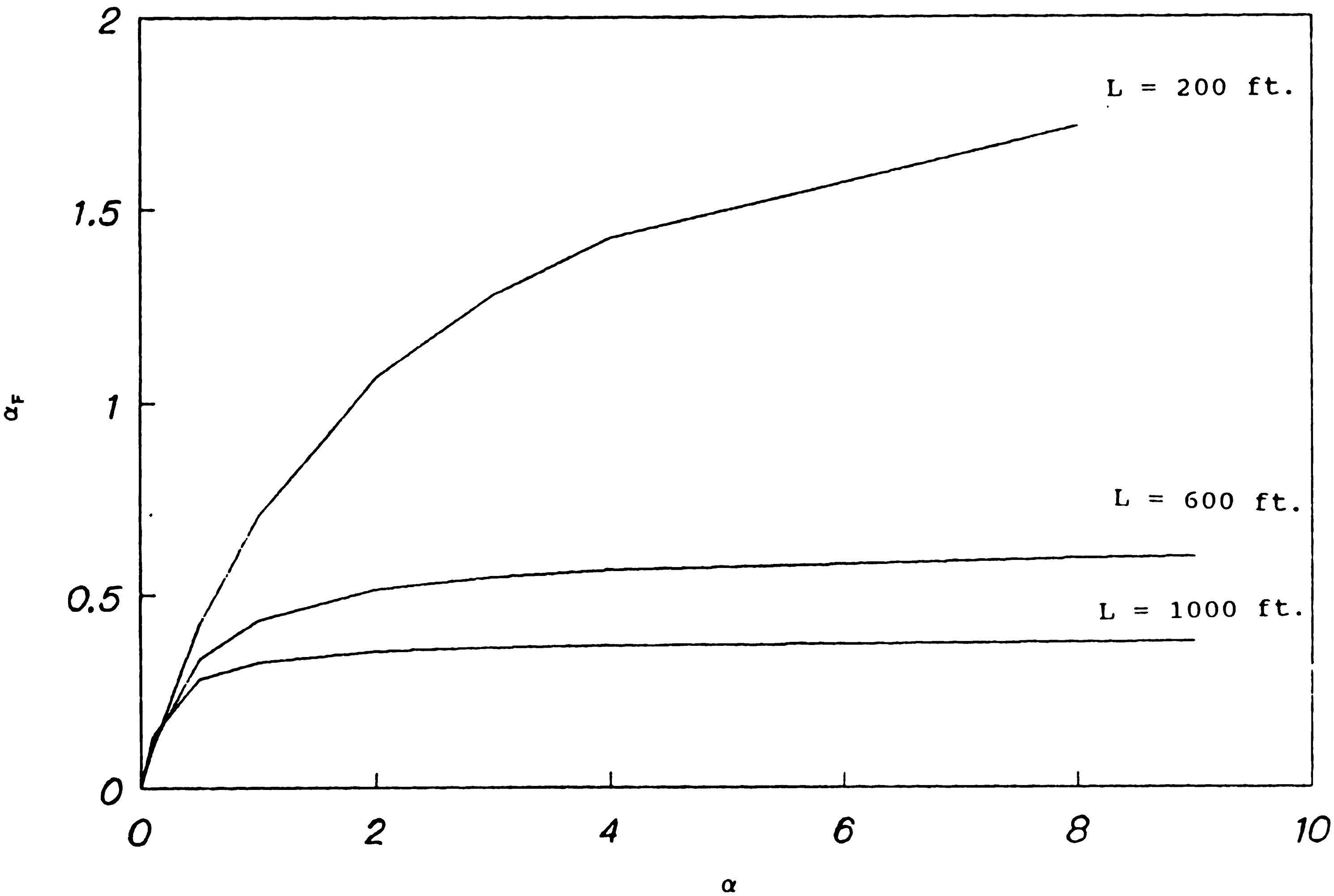

Figure 29 Maximum α_F as a Function of α.

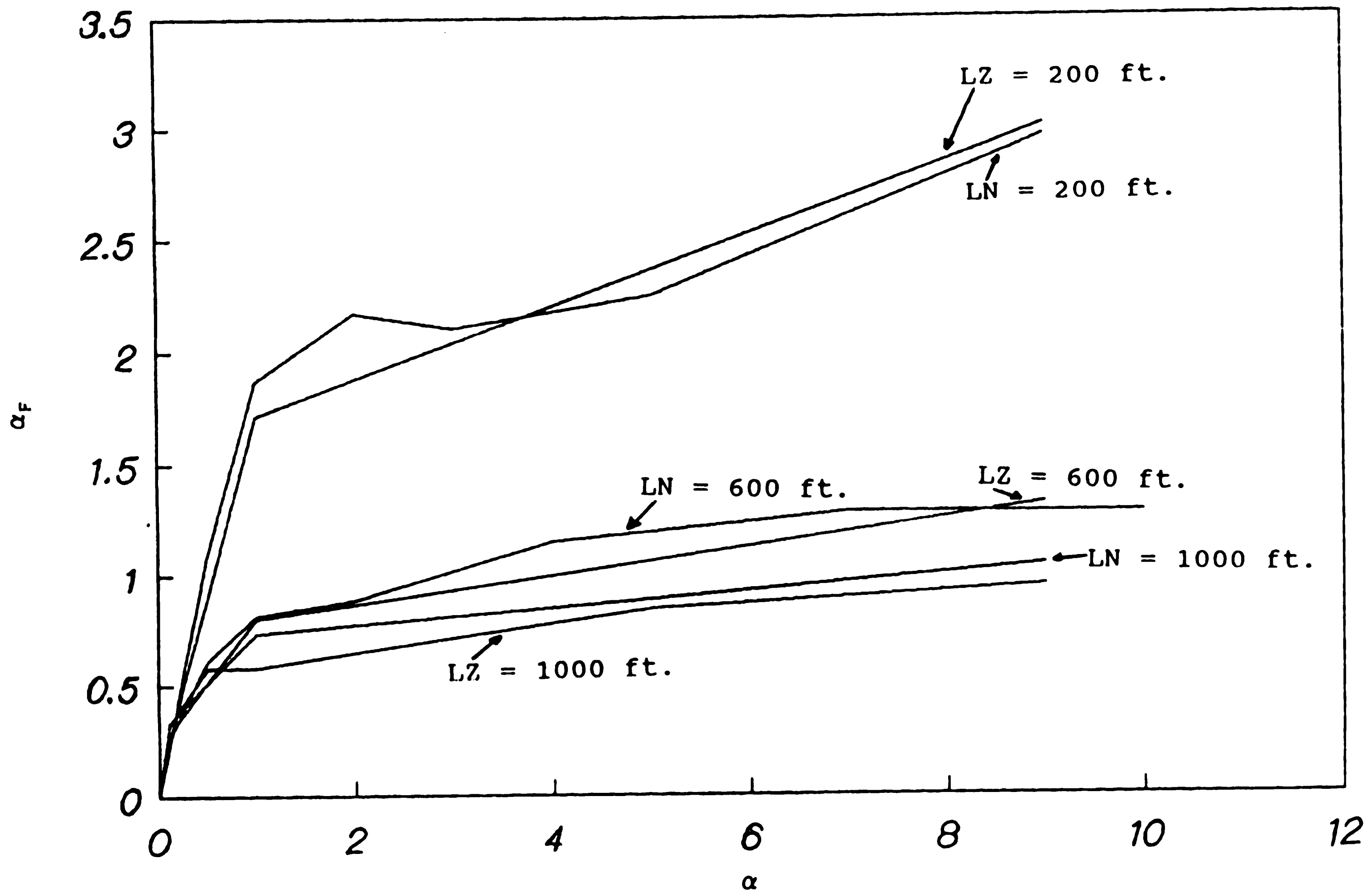

Figure 30 Linear and Linearized Analysis (L = 200 ft., 600 ft., 1000 ft.).

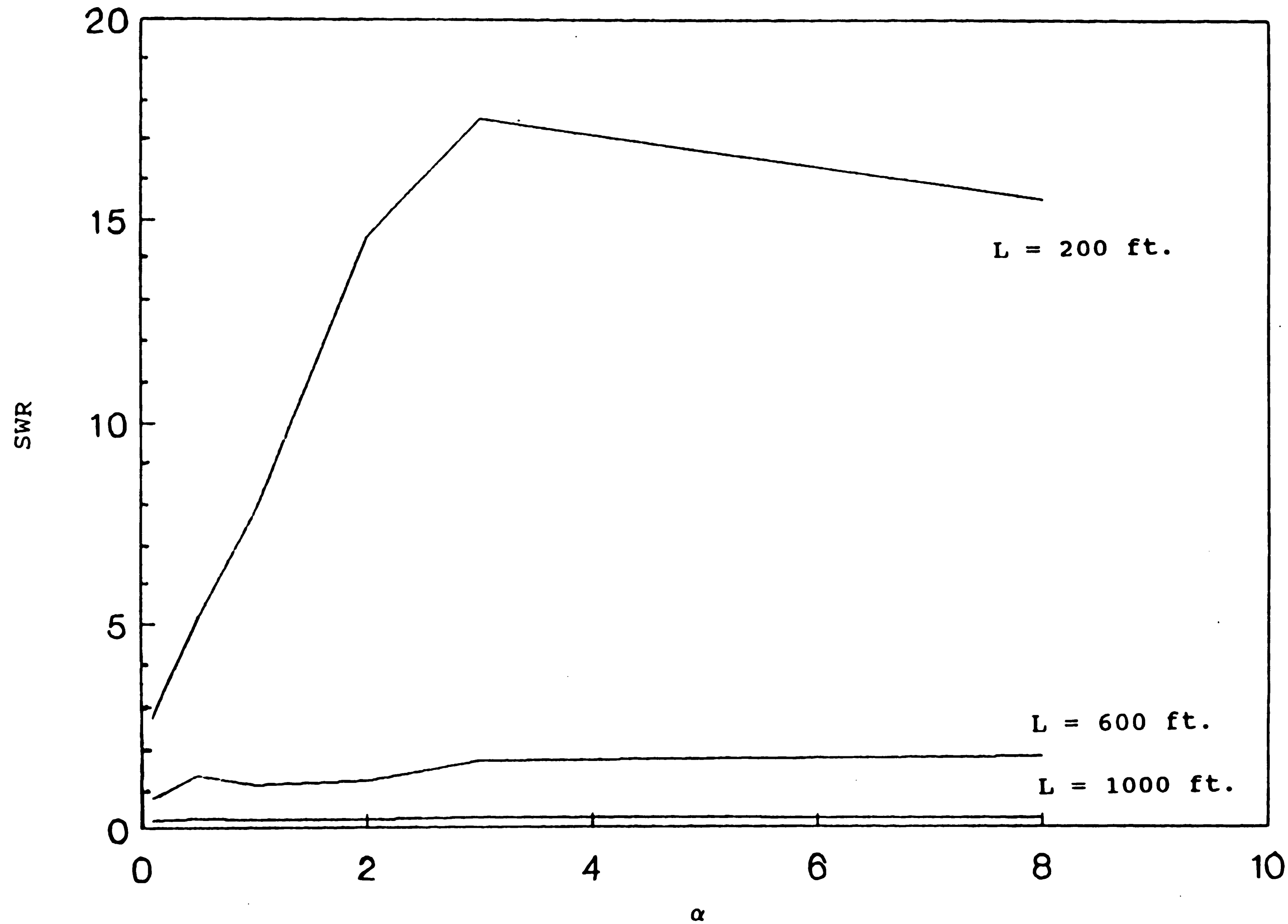

Figure 31 Effect of α on SWR (L = 200 ft., 600 ft., 1000 ft.).

LIST OF REFERENCES

LIST OF REFERENCES

1. Dusseau, R.A., "Seismic Analysis of Two Steel Deck Arch Bridges," M.S. Thesis, Department of Civil Engineering, Michigan State University, 1981.

2. Dusseau, R.A., and Wen, R.K., "Responses of a Long Span Arch Bridge to Differential Abutement Motions", Proceedings of the Third U.S. National Conference on Earthquake Engineering, Charleston, South Carolina, August 1986.

3. Dusseau, R.A., and Wen, R.K., "Seismic Responses of Deck-Type Arch Bridges," Earthquake Engineering and Structural Dynamics, Vol. 18, 1989, pp. 701-715.

4. Kuranishi, S., and Nakajima, A., "Strength Characteristics of Steel Arch Bridges Subjected to Longitudinal Acceleration", Structural Engineering Earthquake Engineering, JSCE, Vol. 3, 1986, pp. 2875-2955.

5. Lee, C.M., "Nonlinear Seismic Analysis of Steel Arch Bridges," Ph.D. Dissertation, Michigan State University, E. Lansing, MI, 1990.

6. Medallah, K., and Wen, R.K., "Elastic Stability of Deck-Type Arch Bridges," Journal of Structural Engineering, ASCE, Vol. 113, No. 4, April 1987, pp. 757-768.

7. Merrit, F., "Structural Steel Designers' Handbook", McGraw-Hill Book Co.,New York, 1972, pp. 13-1-13-41.

8. Raithel, A., and Franciosi, C., "Dynamic Response of Arches Using Lagrangian Approach", Journal of Structural Engineering, April 1984, pp. 847-858.

9. Standard Specifications For Highway Bridges 1983. American Association of State Highway and Transportation Officials. Section 3.15. Washington, D.C.

10. Thakkar, S.K., and Arya, A., "Dynamic Response of Arches Under Seismic Forces", Proceedings of the Fifth World Conference on Earthquake Engineering, Rome, Italy, 1973.

LIST OF REFERENCES (Continued)

11. Wen, R.K., Notes on research. 1/5/91.

12. Wen, R.K., "Seismic Behavior and Design of Arch Bridges," Proceedings of the 4th U. S. National Conference On Earthquake Engineering, Palm Springs, California,May 1990, Vol. 1, pp. 1027-1036.

13. Wen, R.K., and Suhendro, B., "Nonlinear Curved-Beam Element for Arch Structures", Journal of Structural Engineering, Vol. 117, No. 11, Nov. 1991, pp. 3496-3515.

14. U.S. Department of Transporation, "Arch Bridges,"Series No. 2, Washington D.C., 1977.

APPENDIX

GLOSSARY OF SYMBOLS

APPENDIX

GLOSSARY OF SYMBOLS

A = cross-sectional area

Ac = ground acceleration coefficient

A_b = area of cross beam

AF = amplification factor

A_r = cross-sectional area of the rib

A_s = cross-sectional area of the deck stringers

A_x = cross-sectional area of the rib cross-bracing

C_s = seismic response coefficient

c_x = one half of the width of the rib cross-section

c_y = one half of the depth of the rib cross-section

D_{tr} = the maximum tower Z-displacement to the maximum arch crown Z-displacement

D_z = Z-displacement

E = Young's modulus

F = force

g = acceleration of gravity

H = rise (height)

I_{yb} = moment of inertia about cross beam local y-axis

I_{xb} = moment of inertia about cross beam local x-axis

GLOSSARY OF SYMBOLS (Continued)

I_{xr} = moment of inertia about rib local x-axis

I_{yr} = moment of inertia about rib local y-axis

k = stiffness

K_{tb} = torsional constant of the cross beam

L = span length

M = total mass per foot of span length

Mr = mass of the rib total mass

M_y = the bending moment about y-axis

M_x = the bending moment about x-axis

N = number of panels

P = compressive force

R = dynamic response

R_{ST} = static response

r_x = radius of gyration about rib local x-axis

r_y = radius of gyration about rib local y-axis

S = section modulus

S = dimensionless soil coefficient

SAM = ratio of axial stress to total stress

SF_{site} = scaling factor

SR = maximum stress ratio (dynamic stress to static stress)

SWR = ratio of the seismic stress to the wind stress

SYM = ratio of stress due to bending moment about the y-axis to total stress

SXM = ratio of stress due to bending moment about the x-axis

GLOSSARY OF SYMBOLS (Continued)

to total stress

T = period of the bridge

T_{in} = fundamental in-plane period

T_{out} = fundamental out-of-plane period

W = width of the bridge

X, Y, Z = global coordinate axes in the x, y, and z direction

X-bracing = cross-bracing

X-beams = cross-beams

x_g = ground acceleration in the X-direction

y_g = ground acceleration in the Y-direction

z = displacement in Z-direction

Z-force = force in the Z-direction

z_g = ground acceleration in the Z-direction

α = ratio of end tower lateral stiffness to rib system lateral stiffness

α_F = ratio of the Z-force through a single tower to the Z-force through the rib system

ξ = critical damping coefficient

Σ_{total} = total stress